Synthesis of Nanoparticles and Surface Modifications

Self-Assembly

- Static assembly
- Dynamic assembly
  - RT = 8.314 J/mol x 300 = 2.4 kJ/mol
- Driving forces
  - Chemisorption
  - Surface effect
  - Hydrophobic-hydrophilic
  - Intermolecular forces
  - Capillary force

Langmuir-Blodgett Films

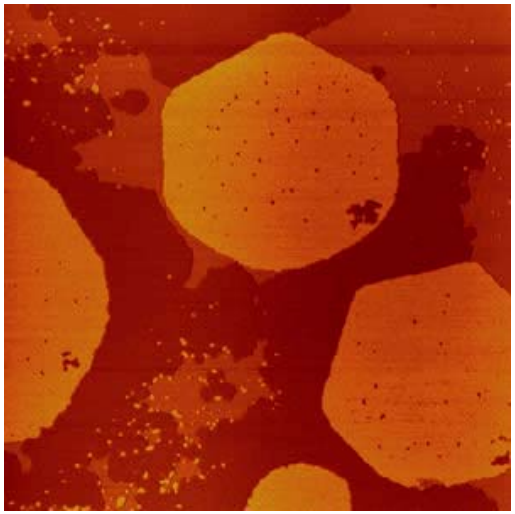

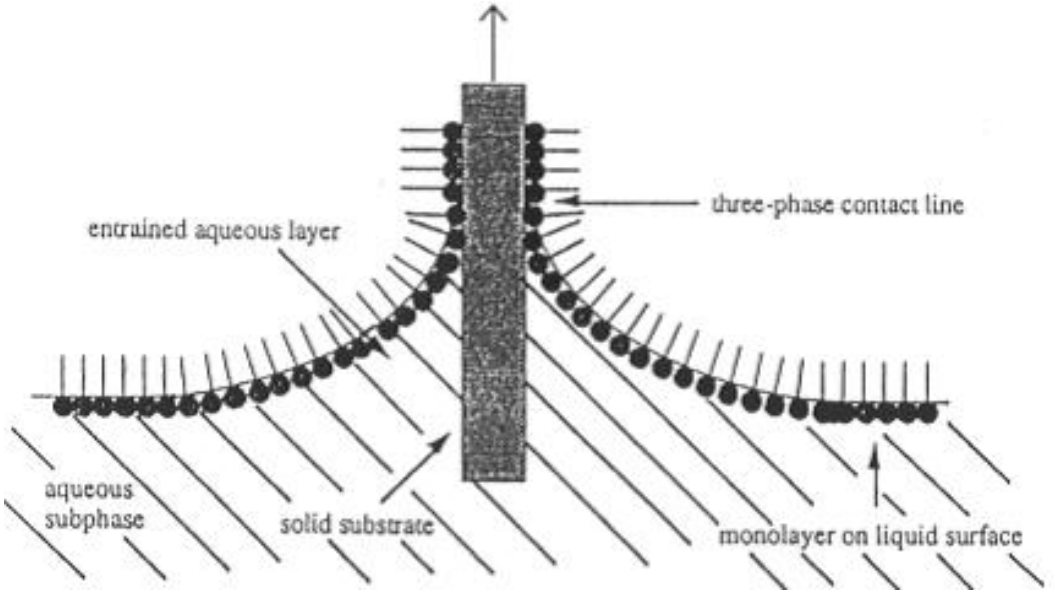

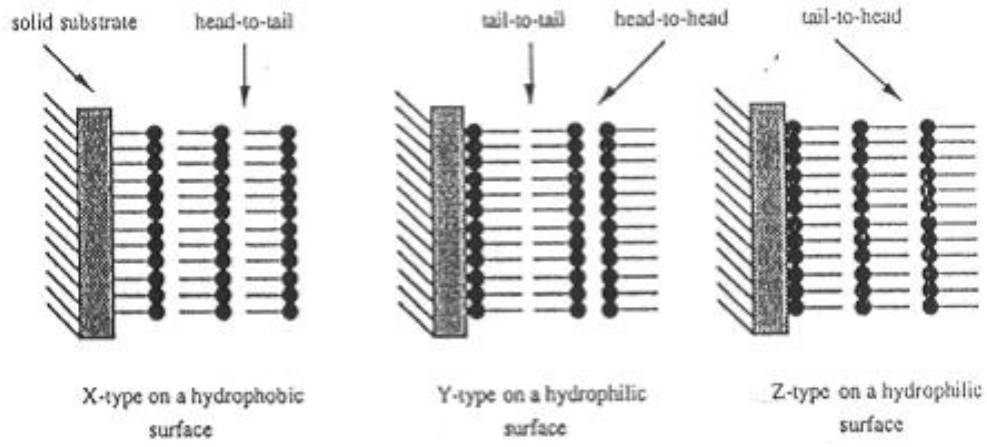

Langmuir-Blodgett Films

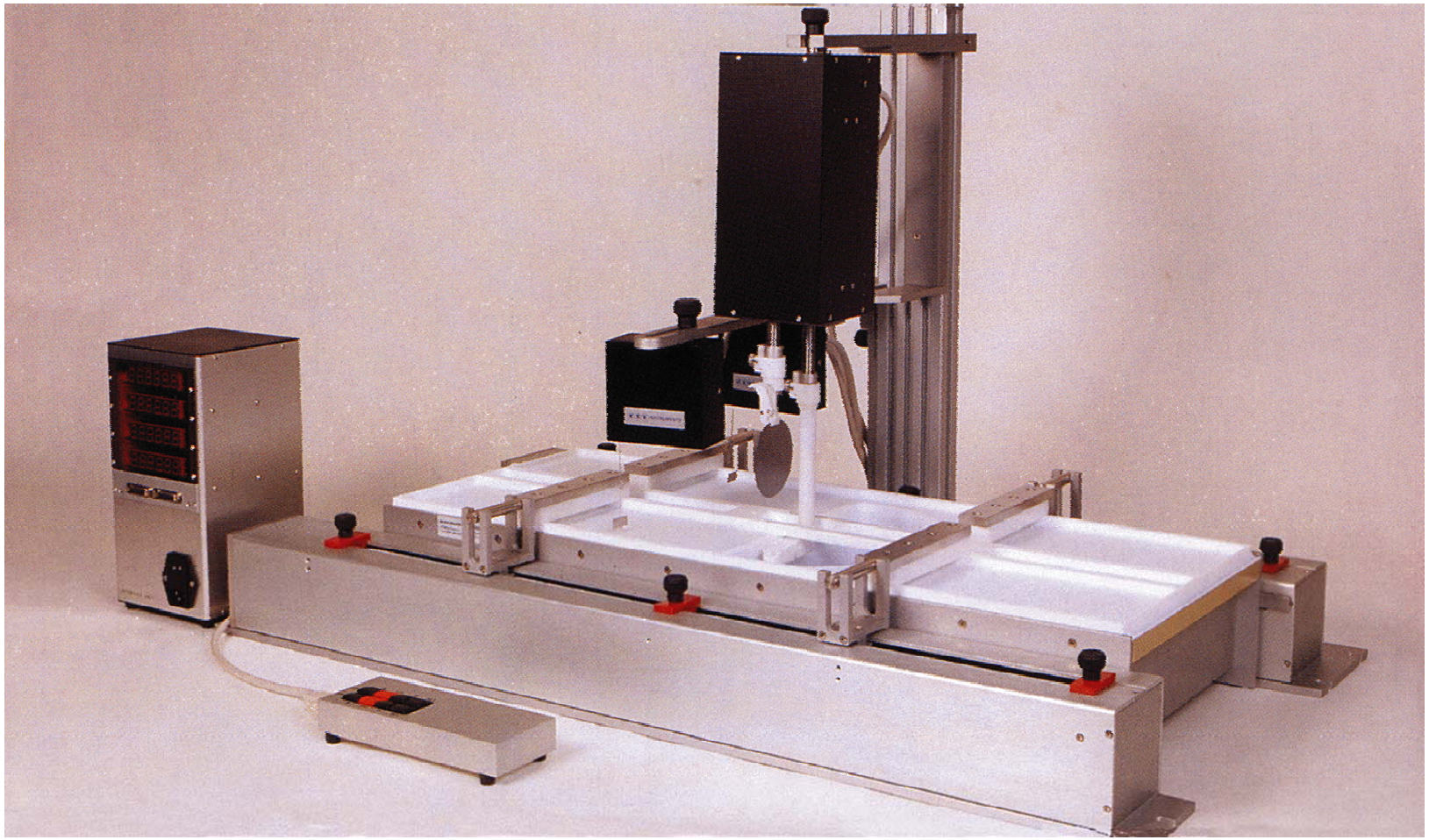

Isotherm

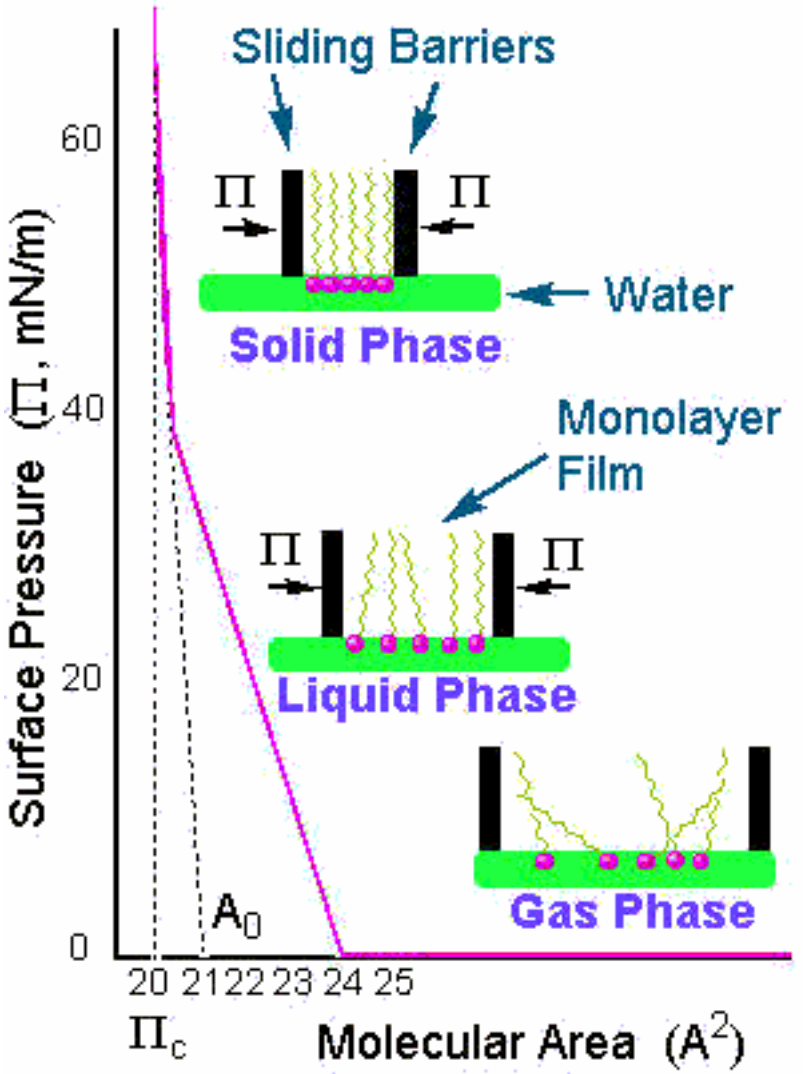
Sliding Barriers
Π
Π
Water
Solid Phase
Monolayer
Film
Π
Π
Liquid Phase
Gas Phase
A0
Surface Pressure (Π, mN/m)
60
40
20
0
20 21 22 23 24 25
Πc
Molecular Area (A2)

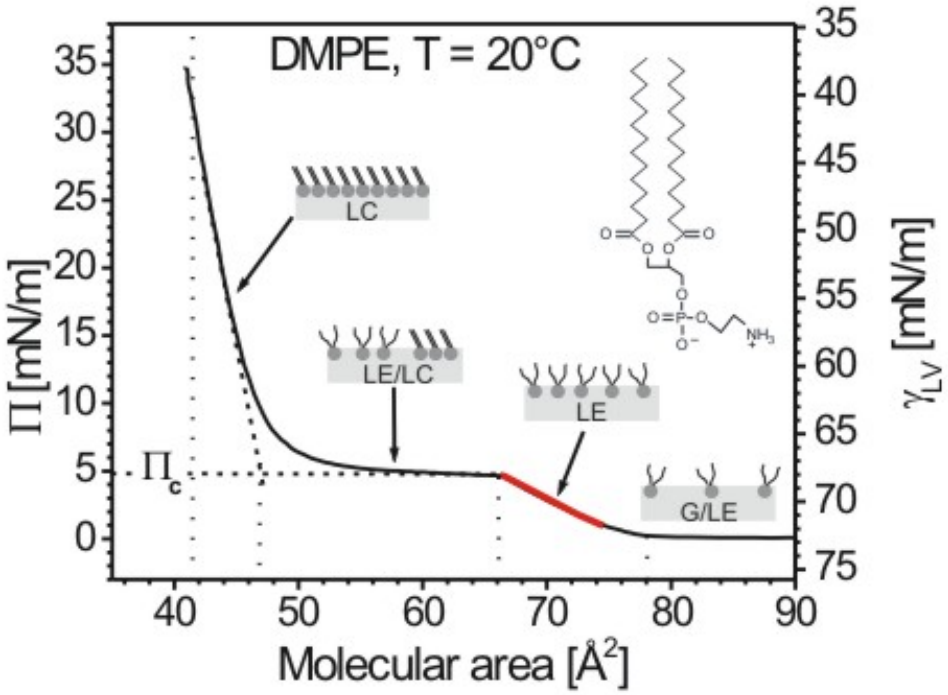
DMPE, T = 20°C
LC
LE/LC
LE
G/LE
Πc
Π [mN/m]
γLV [mN/m]
35
30
25
20
15
10
5
0
40
45
50
55
60
65
70
75
40
50
60
70
80
90
Molecular area [Å2]

Self-Assemble Monolayer (SAM)

Chem. Rev. **2005**, *105*, 1103–1169

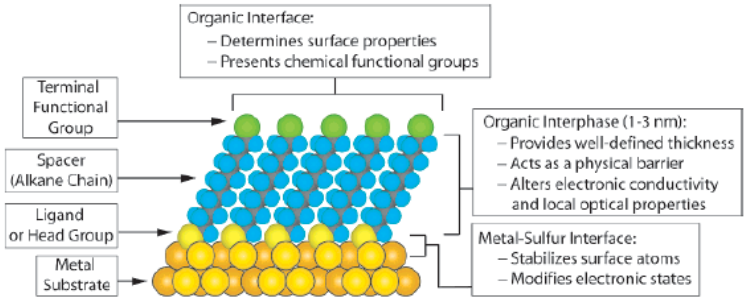

Ligand	Substrates	Morphology of Substrate: Thin Films or Bulk Material	Morphology of Substrate: Nanoparticles or Other Nanostructures
ROH	Fe_xO_y		35
	Si-H	36	
	Si	37	
RCOO-/RCOOH	α-Al_2O_3	38,39	
	Fe_xO_y		40
	Ni		41,42
	Ti/TiO_2	43	
RCOO–OOCR	Si(111):H	44	
	Si(100):H		
Ene-diol	Fe_2O_3		45
RNH_2	FeS_2	46	
	Mica	47	
	Stainless Steel 316L	48	
	$YBa_2Cu_3O_{7-\delta}$	49	
	CdSe		50
RC≡N	Ag	51	
	Au		
R-N≡N$^+$(BF_4^-)	GaAs(100)	52	
	Pd	52	
	Si(111):H	52	
RSH	Ag	26	53,54
	$Ag_{90}Ni_{10}$	55	
	AgS		56
	Au	26	57
	AuAg		58
	AuCu		58
	Au_xPd_{1-x}		58
	CdTe		59
	CdSe		60
	CdS		61,62
	Cu	26	58
	FePt		63-66
	GaAs	67	
	Ge	68	
	Hg	69-71	
	HgTe		72
	InP	73	
	Ir		74
	Ni	75	
	PbS		76-78
	Pd	30	74,79
	PdAg		58
	Pt	32	80
	Ru		81
	Stainless Steel 316L	48	
	$YBa_2Cu_3O_{7-\delta}$	82	
	Zn	83	
	ZnSe	84	
	ZnS		85
RSAc	Au	86	
R–S	Au		87
RSR'	Au	88	

Ligand	Substrates	Morphology of Substrate: Thin Films or Bulk Material	Morphology of Substrate: Nanoparticles or Other Nanostructures
RSSR'	Ag	89	90
	Au	20	90-92
	CdS		61
	Pd	30	
	Au	93	
RCSSH	Au	94	
	CdSe		95
$RS_2O_3^-Na^+$	Au	96	98
	Cu	97	
RSeH	Ag	99	
	Au	100,101	
	CdS		60
	CdSe		102
RSeSeR'	Au	101	
R_3P	Au		103
	FeS_2	46	
	CdS		104
	CdSe		104
	CdTe		104
$R_3P=O$	Co		105,106
	CdS		104
	CdSe		104
	CdTe		104
$RPO_3^{2-}/RP(O)(OH)_2$	Al	107	
	Al-OH	108	
	$Ca_{10}(PO_4,CO_3)_6(OH)_2$	109	
	GaAs	110	
	GaN	110	
	Indium tin oxide (ITO)	111	
	Mica	112	
	TiO_2	113,114	
	ZrO_2	114,115	
	CdSe		116-118
	CdTe		118,119
RPO_4^{2-}	Al_2O_3	120	
	Nb_2O_5	120	
	Ta_2O_3	121	
	TiO_2	120,122	
RN≡C	Pt	123	124
$RHC=CH_2$	Si	37	
RC≡CH	Si(111):H	125	
$RSiX_3$ X = H, Cl, OCH_2CH_3	HfO_2	126	
	ITO	127	
	PtO	128	
	TiO_2	113,126,129	
	ZrO_2	126,129	

S-Au 25-30 Kcal/mole
Si-O 190 kcal/mole

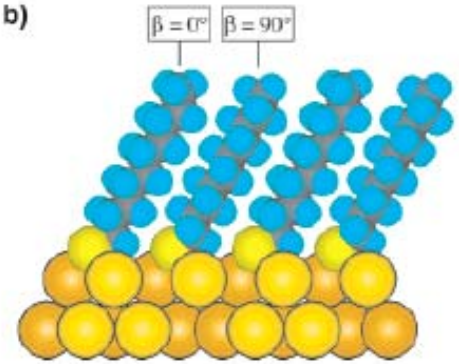

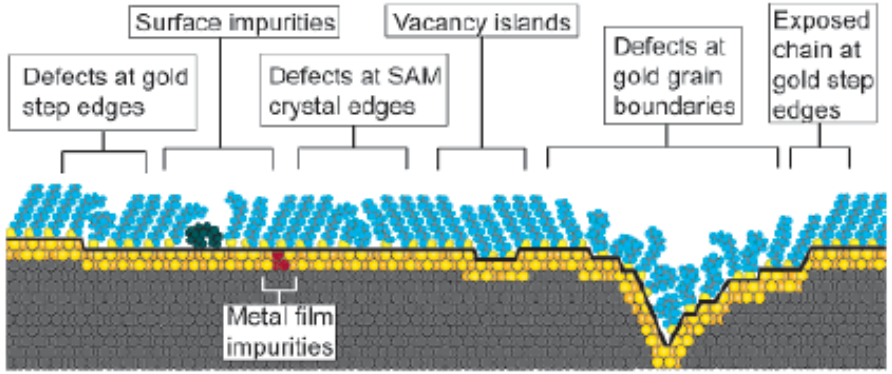

Figure 7. Schematic illustration of some of the intrinsic and extrinsic defects found in SAMs formed on polycrystalline substrates. The dark line at the metal−sulfur interface is a visual guide for the reader and indicates the changing topography of the substrate itself.

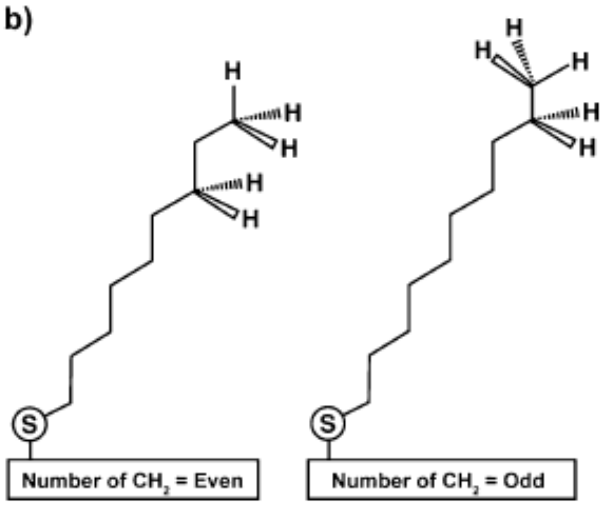

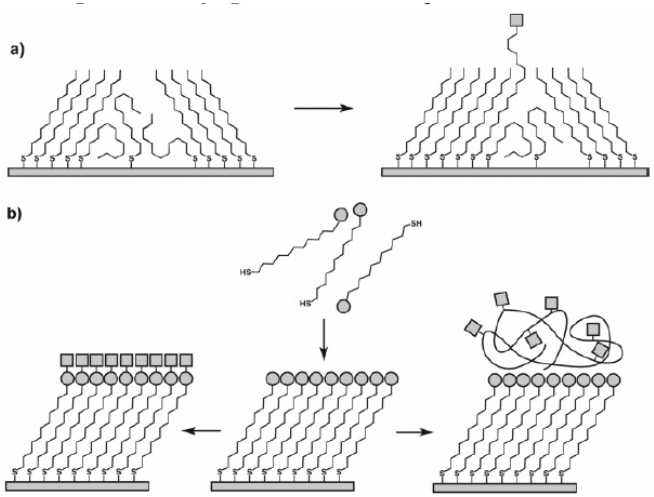

[c] (a) Insertion of a functional adsorbate at a defect site in a preformed SAM. (b) Transformation of a SAM with exposed functional groups (circles) by either chemical reaction or adsorption of another material.

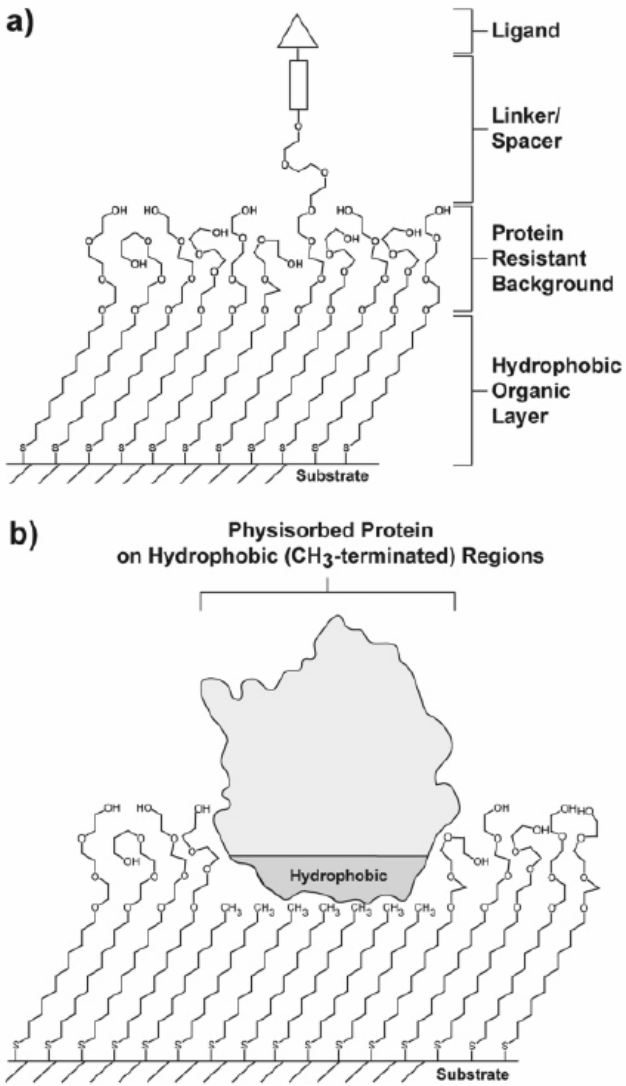

Figure 21. Schematic illustrations of (a) a mixed SAM and (b) a patterned SAM. Both types are used for applications in biology and biochemistry.

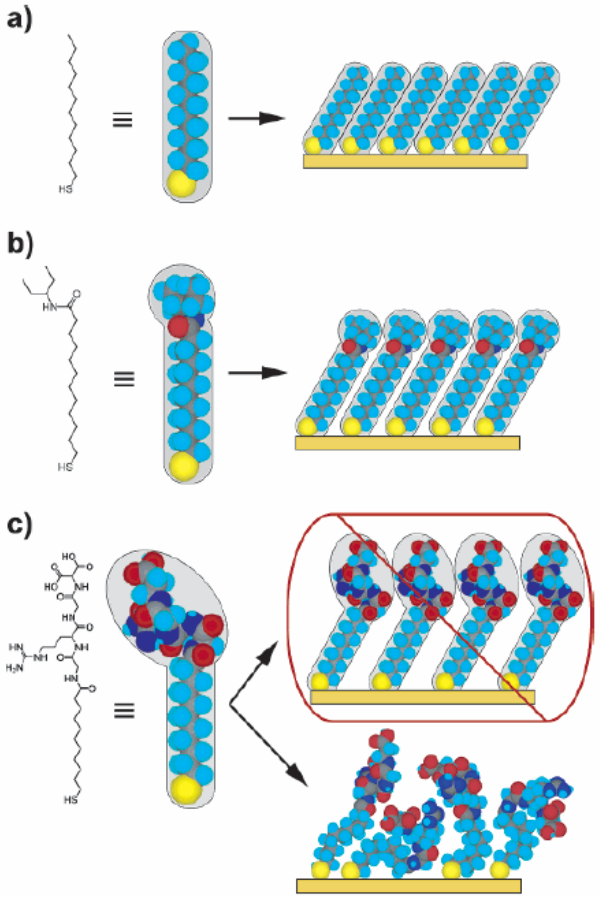

Figure 22. Schematic diagram illustrating the effects that large terminal groups have on the packing density and organization of SAMs. (a) Small terminal groups such as $-CH_3$, $-CN$, etc., do not distort the secondary organization of the organic layer and have no effect on the sulfur arrangement. (b) Slightly larger groups (like the branched amide shown here) begin to distort the organization of the organic layer, but the strongly favorable energetics of metal−sulfur binding drive a highly dense arrangement of adsorbates. (c) Large terminal groups (peptides, proteins, antibodies) sterically are unable to adopt a secondary organization similar to that for alkanethiols with small terminal groups. The resulting structures probably are more disordered and less dense than those formed with the types of molecules in a and b.

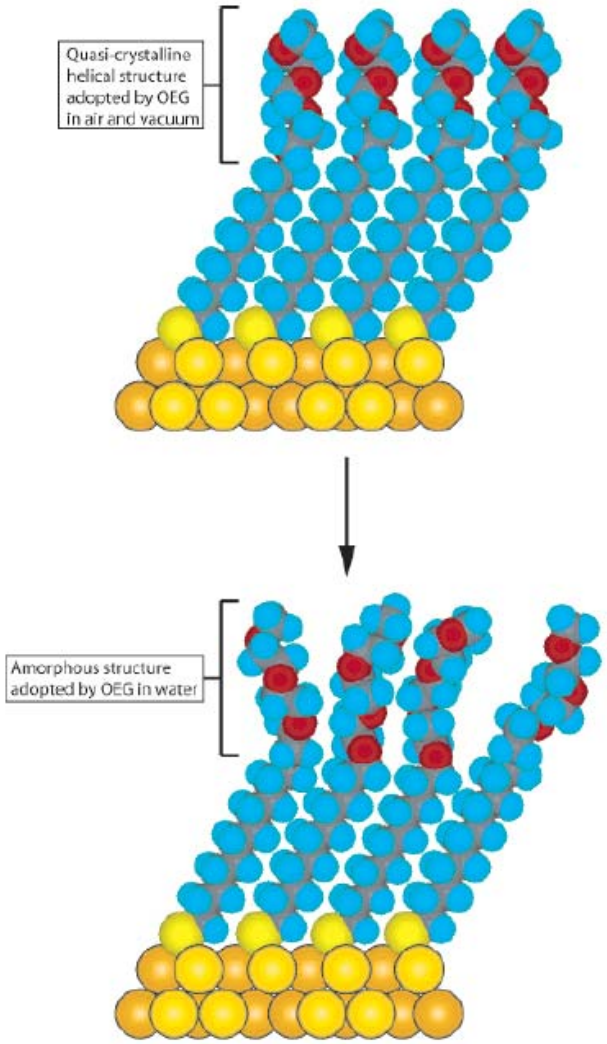

Figure 23. Schematic illustration of the order−disorder transition evidenced by SAMs of alkanethiolates terminated with triethylene glycol. The EG_3 group loses conformational ordering upon solvation in water.

Temperature Programmed Desorption

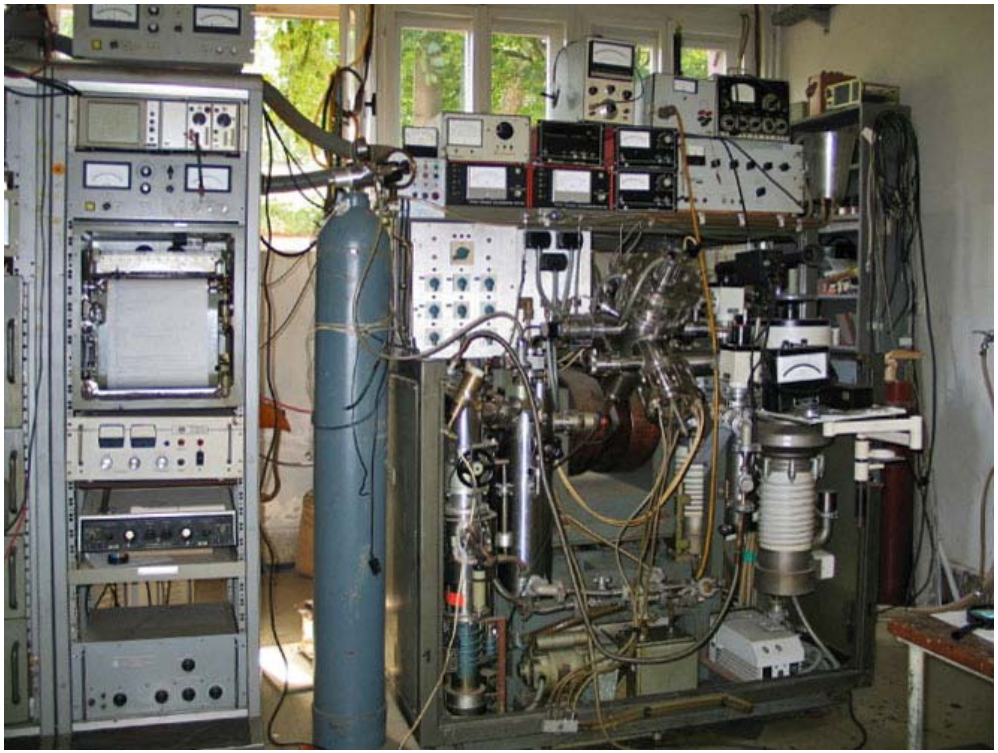

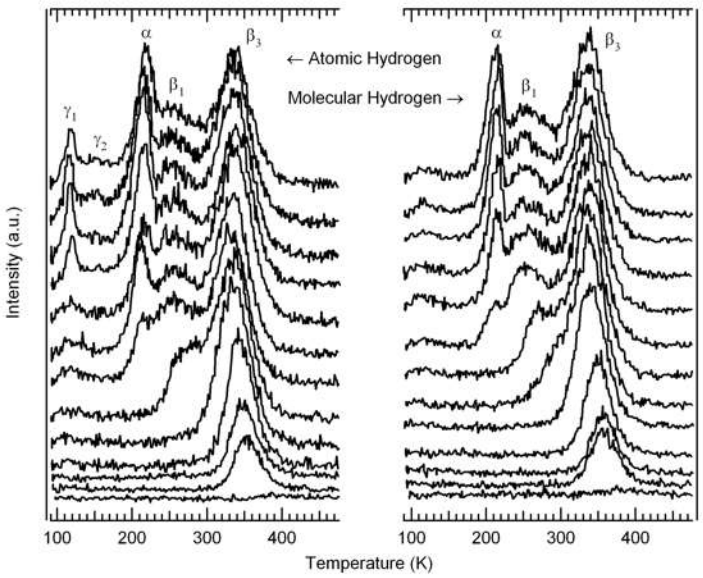

Self-Assembly

- Substrates
- Interstitial adhesion layer
- Noble metal layer
- Organo-sulfur

Organosilanes

Self-assembled monolayers

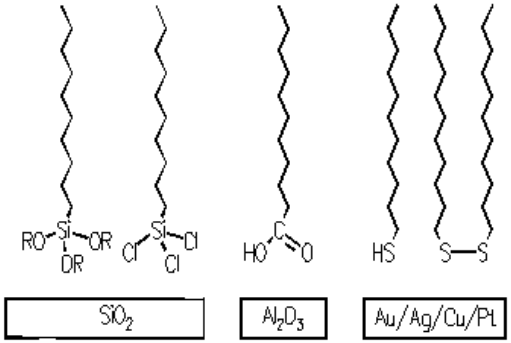

- Surface
- silicon oxide: silanisation
- aluminum oxide: fatty acids
- metals: thiols and sulfides

Immersion of substrate in a solution containing the adequate molecules for 12 - 24 hours yields an ordered monolayer

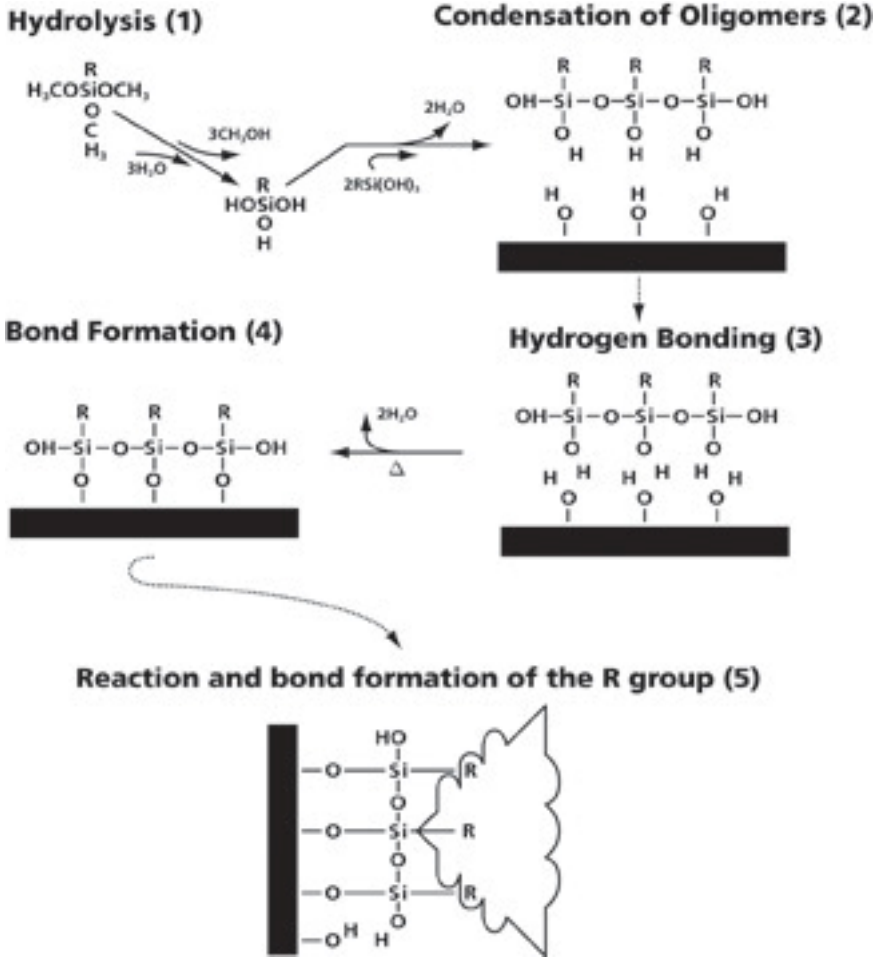

Metal Reduction

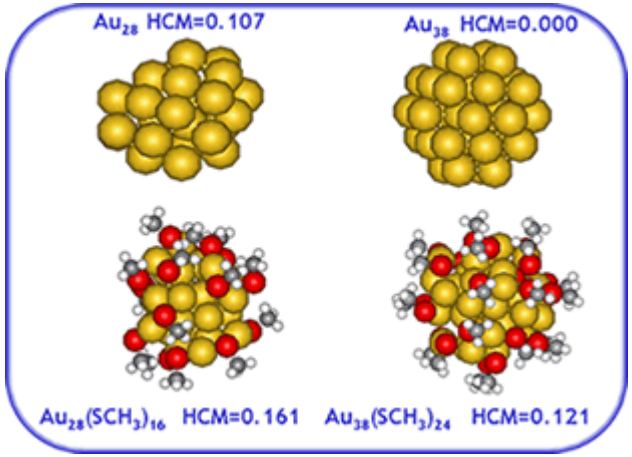

Synthesis of Silver Nanoparticles

1. ***A solution of $AgNO_3$ (1.0×10^{-3} M) in deionized water was heated until it began to boil.***
2. ***Sodium citrate solution was added dropwise to the silver nitrate solution as soon as the boiling commenced. The color of the solution slowly turned into grayish yellow, indicating the reduction of the Ag+ ions.***
3. ***Heating was continued for an additional 15 min, and then the solution was cooled to room temperature before employing for further experimentation.***

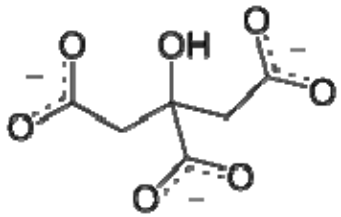

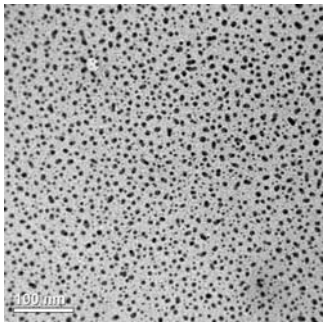

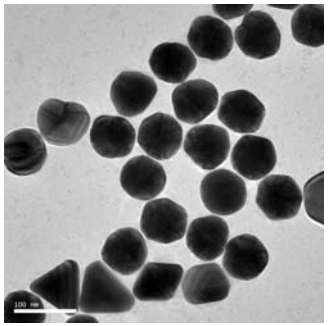

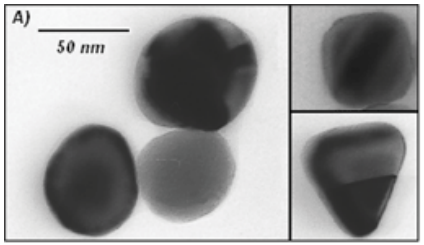

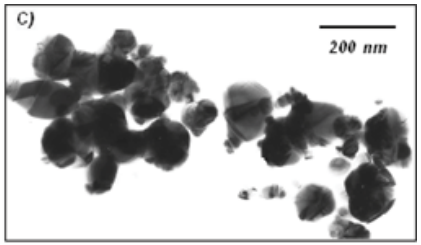

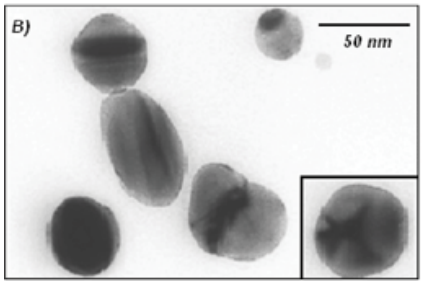

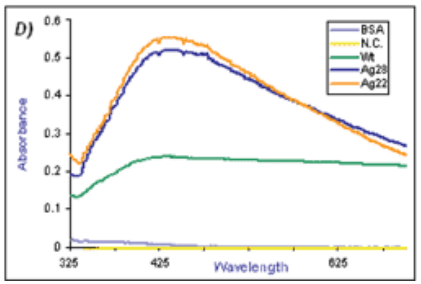

Synthesis of Gold Nanoparticles

1. ***Add 20 mL of 1.0 mM $HAuCl_4$ to a 50 mL round bottom flask on a stirring hot plate.***
2. ***Add a magnetic stir bar and bring the solution to a boil.***
3. ***To the boiling solution, add 2 mL of a 1% solution of trisodium citrate dihydrate***
4. ***The gold sol gradually forms as the citrate reduces the gold(III). Stop heating when a deep red color is obtained.***

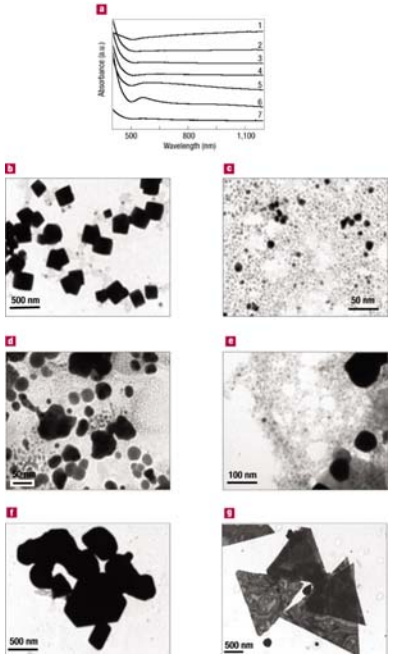

(1) $$M_xO_y \xrightarrow[(\text{medium})\ \Delta_T]{\text{Reducing Agent}} M_n + H_2O$$

(Reducing Agent = R - COH)

(2) $$M(L)_x \xrightarrow[(\text{medium})\ \Delta_T]{\text{Reducing Agent}} M_n + L^-$$

($L=NO_3^-, C_2H_5O^-$)

(Reducing Agent = R - COH)

Construction of Core Shell Ag/Au@SiO_2 Nanoparticles

1. *Under vigorous stirring, 1 ml of the silver/ gold colloids solution was mixed with 250 mL of isopropanol and 25 mL of deionized water.*
2. *Immediately after the addition of 4 mL of 30% ammonium hydroxide, different amounts of tetraethoxysilane (TEOS) were added to the reaction mixture.*
3. *To obtain different silica layer thicknesses, TEOS solutions with a concentration between 50% and 100% was added to the suspension. The reaction was stirred at room temperature for 30 minutes and then was allowed to age without agitation at 4 ℃ overnight.*
4. *Each suspension of silica-coated silver/gold nanoparticles was washed and centrifuged, followed by re-suspension in water. The thickness of the silica layers was determined from TEM images .*

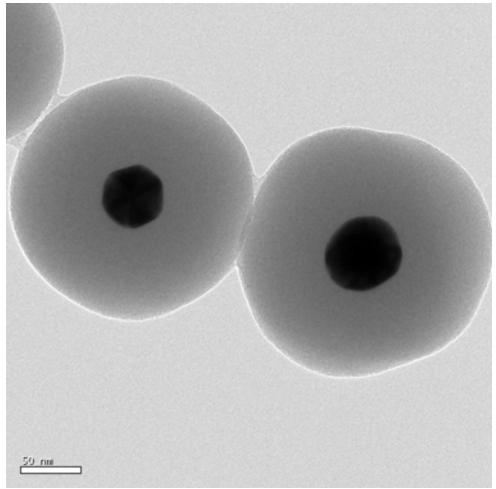

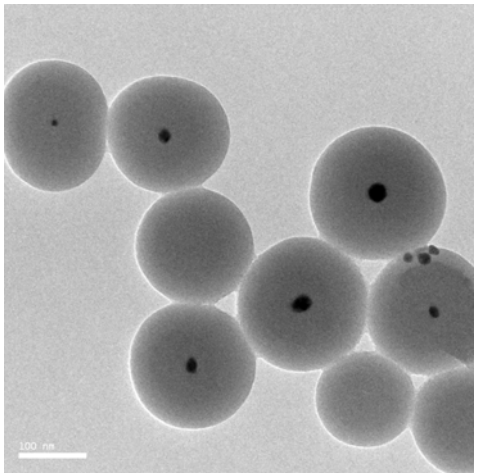

Core-Shell Nanoparticles

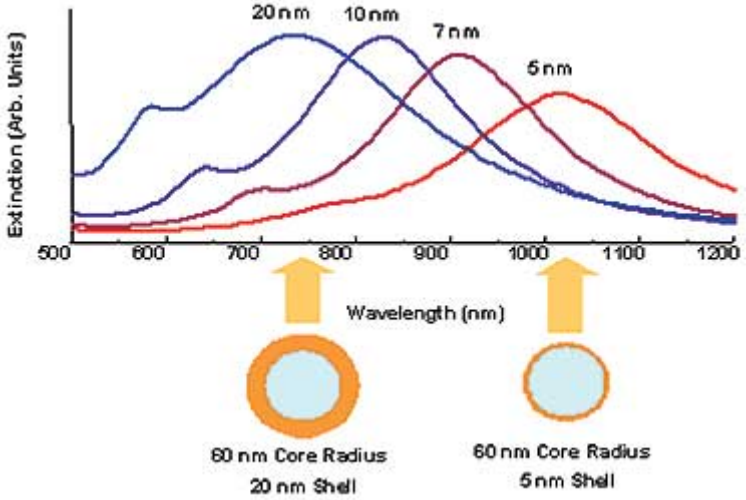

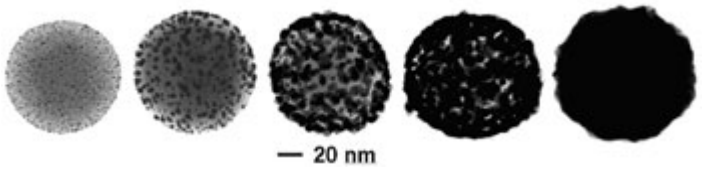

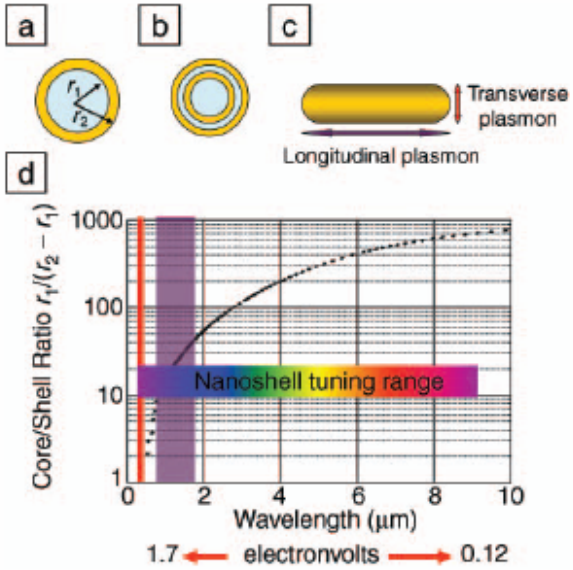

Figure 1. (a) Schematic illustration of a silica-core, gold-shell nanoshell, indicating inner (r_1) and outer (r_2) radii of the shell layers. (b) Depiction of a four-layer, concentric nanoshell. (c) Schematic illustration of a metallic nanorod. (d) Plot of nanoshell resonance as a function of core and shell dimensions, overlaid with reported spectral ranges of nanorod resonances (red, transverse plasmon; purple, longitudinal plasmon), and reported nanoshell and concentric nanoshell combined spectral range of plasmon response.

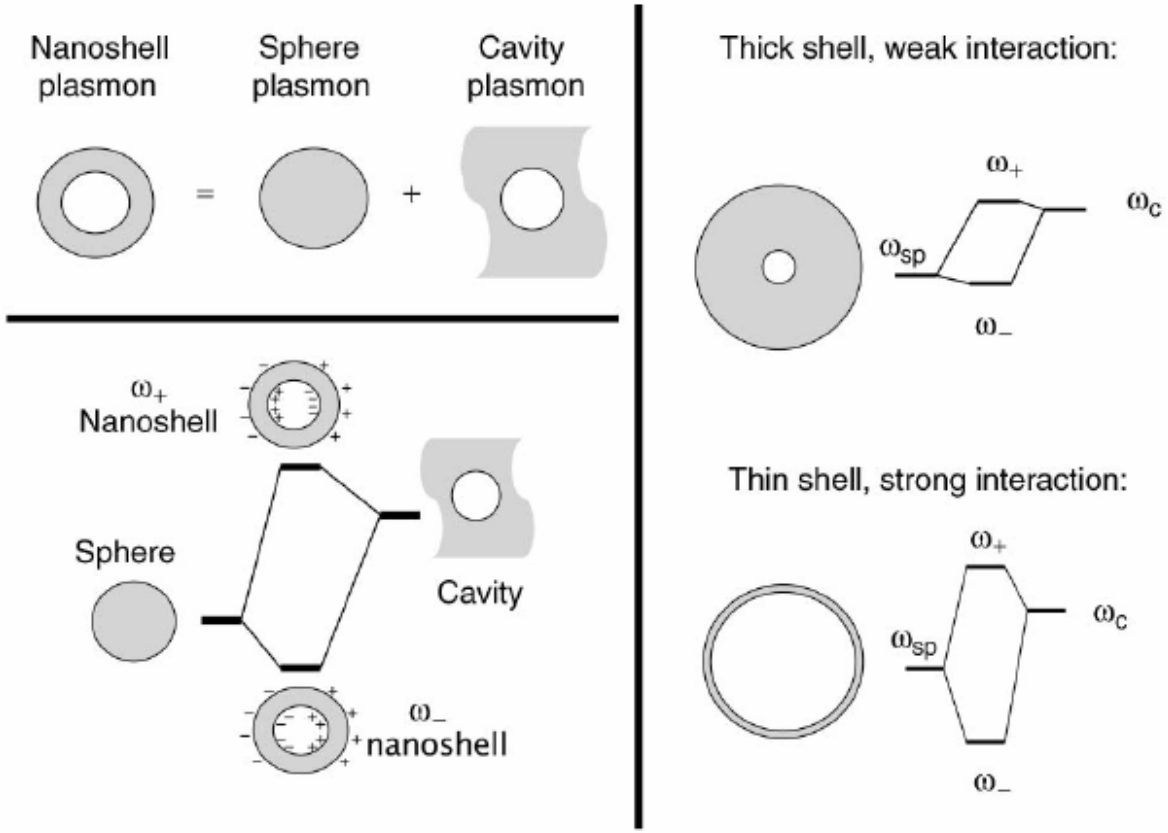

Figure 2. Plasmon hybridization and the sphere–cavity model for nanoshells: the interaction between a sphere (resonance frequency, ω_{sp}) and a cavity plasmon (resonance frequency, ω_c) is tuned by varying the thickness of the shell layer of the nanoparticle. Two hybrid plasmon resonances, the ω_- "bright," or "bonding," plasmon and the ω_+ "dark," or "anti-bonding," plasmon resonances are formed. The lower-energy plasmon couples most strongly to the optical field.

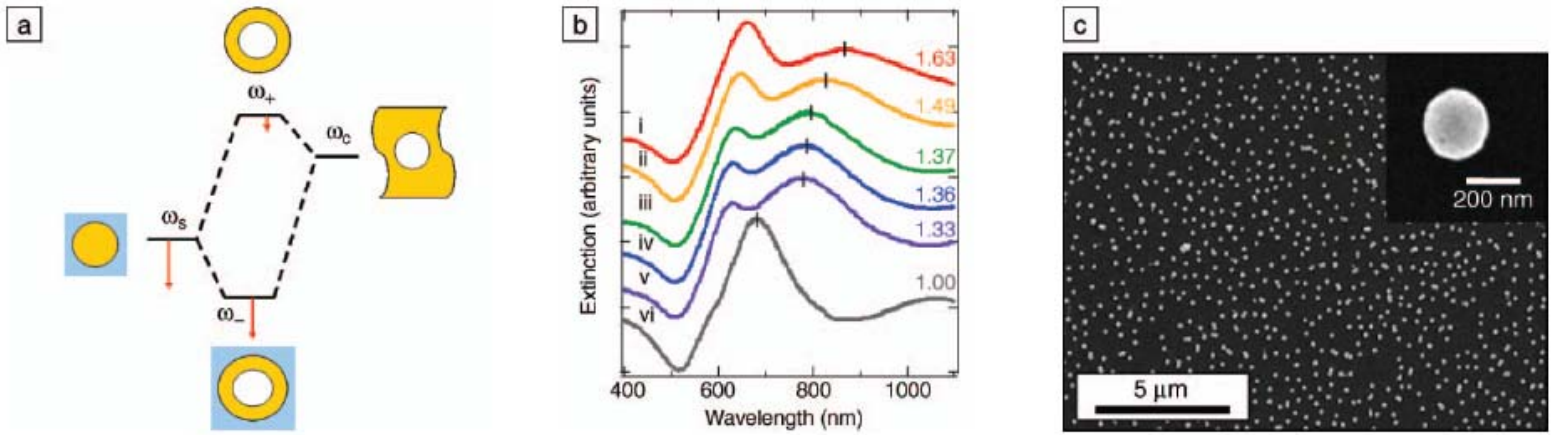

Figure 5. (a) Plasmon hybridization picture applied to surface plasmon resonance sensing with nanoshells: the low-energy "bonding" plasmon, ω_-, is sensitized to changes in its dielectric environment. The blue background schematically denotes the embedding medium for the nanoparticle. (b) Experimental curves showing plasmon resonance shifts for nanoshell-coated films in various media: (i) carbon disulfide, (ii) toluene, (iii) hexane, (iv) ethanol, (v) H_2O, and (vi) air. The index of refraction for each embedding medium is noted on the far right of the spectra. Spectra are offset for clarity. (c) Scanning electron micrograph of nanoshells deposited onto a poly(vinyl pyridine) functionalized glass surface, as used to acquire data in (b). Inset: individual nanoshell.

Preparation of Fe_3O_4@Ag/Au

1. *To the magnetic nanoparticle suspension obtained from commercial company, add 50 ml of a solution of Au (III) salt or Ag (I) salt at concentration of 0.01–1% mmol/L , shaking for 30 minutes, allowing Au (III) or Ag (I) ion to absorb on the surface of magnetic nanoparticle sufficiently,*
2. *Then adding 15–40 ml of reducing agent, such as hydroxylamine hydrochloride at concentration of 40 mmol/L, reacting for 5–40 minutes.*
3. *Further adding 1–10 ml of a solution of Au (III) salt or Ag (I) salt at concentration of 0.01–1%, shaking for 10 minutes, coating a reduced layer of gold or silver on the surface of the magnetic nanoparticle, forming super-paramagnetic composite particles having core/shell structure, separating magnetically, washing repeatedly with distilled water.*

.

Synthesis of CdSe Quantum Dots

Synthesis of TOPO/HDA capped quantum dots of CdSe

Cadmium acetate (0.107g, 0.4mmol) and oleic acid (0.27mL, 0.4mmol) in 1:2 ratio were placed in a two neck flask degassed and refilled with nitrogen, stirred at 120-130 ^{0}C under nitrogen atmosphere for 2-3 hours, obtained a clear light yellow solution. Then a mixture of capping reagent i.e. 6g of hexadecylamine (HDA) and 6g of tri-octylphosphine oxide (TOPO) prepared in separate flask was added at the same temperature and stirring was done for another 30min at temperature ~ 350 ^{0}C. The temperature was reduced and TOPSe was added at different temperatures at 250 ^{0}C through syringe immediately the color of reaction mixture became dark brown (TOPSe was prepared simultaneously in a separate vessel, appropriate quantity of Se (0.032g) powder was heated in 2mL tri-octyl phosphine (TOP) at 70-90 ^{0}C for about an hour to get a clear solution of TOPSe), stirring was continued for another 30min aliquots were taken from the reaction solution to monitor the reaction. The temperature of the reaction was reduced the stirring was done for another 1-2 hours. 50mL toluene was added before the cooling the reaction to prevent the solidification of TOPO and HDA. It was centrifuged at 3000rpm for 15min, a pallet was discarded, the supernatant solution was treated with the methanol for precipitation of CdSe nano-crystals, centrifuged at 7000rpm washed with methanol (3 x 6mL) to get product. A red residue was obtained which was re-dispersed in toluene.

Synthesis of CdSe Quantum dots

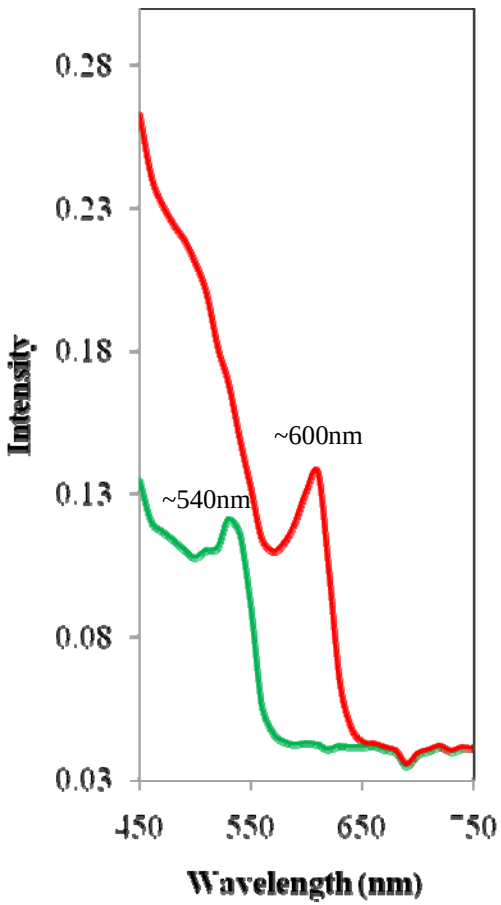

FWHM= ~28nm ± 2

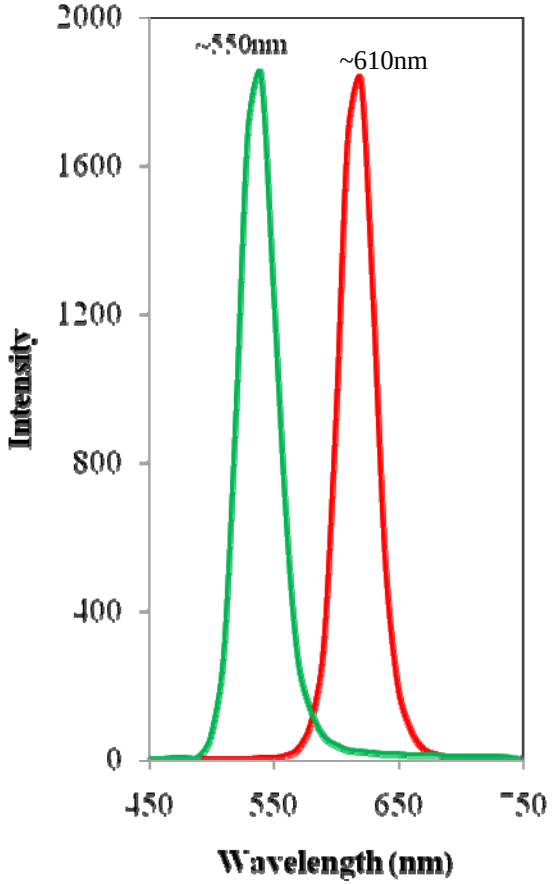

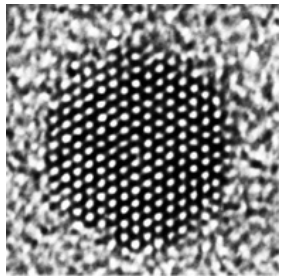

Cooperative UV and PL spectra of CdSe core

Synthesis of CdSe/ZnS Quantum Dots

20mL (31mg, 0.16 mmol) colloidal solution of CdSe QDs from stock solution (54mg dissolved in 35mL toluene) was placed in a two-neck flask. TOPO (6g) and HAD (6g) were added and then toluene was removed through vacuum, flask refilled with nitrogen. The reaction mixture was heated at 350 ^{0}C for two hours. In another flask zinc acetate in 1:3 ratio with respect of CdSe and was dissolved in 4mL of oleic acid stirred at 120 ^{0}C for 2 hours obtained a light yellow coloured solution and temperature reduced to 60-70 ^{0}C. After cooling to room temperature, TOPSe was mixed with Zn salt solution. And the mixture was injected slowly through syringe in to reaction solution of CdSe-TOPO at 180-200 ^{0}C. The stirring was done for another an hour. The similar procedure was followed for work up of reaction as avobe experiment. The final product was re-dispersed in toluene.

Light emission from CdSe/ZnSe Quantum dots

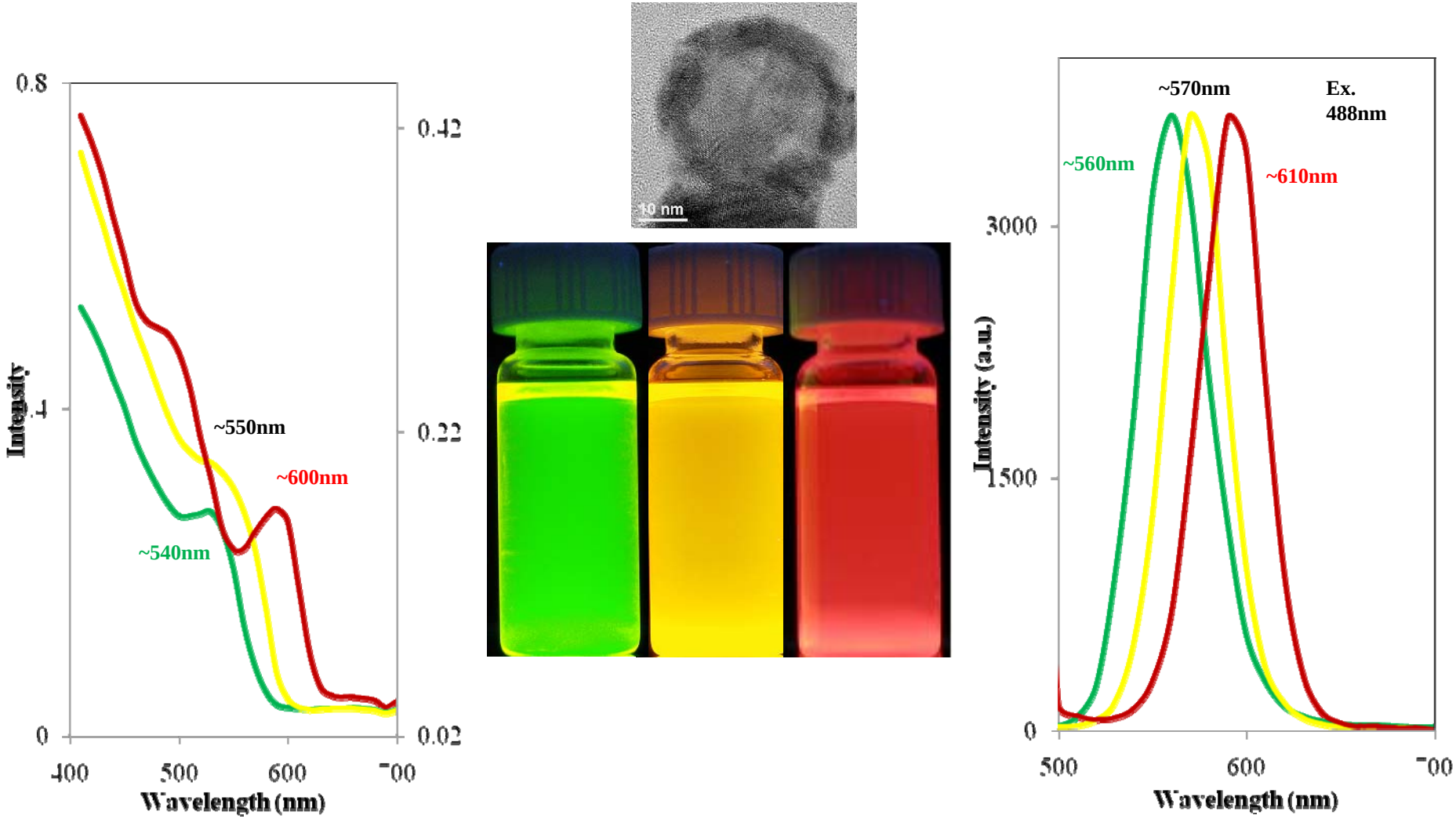

UV-Visible and PL spectra of CdSe/ZnSe re-dispersed in toluene

Nanorods

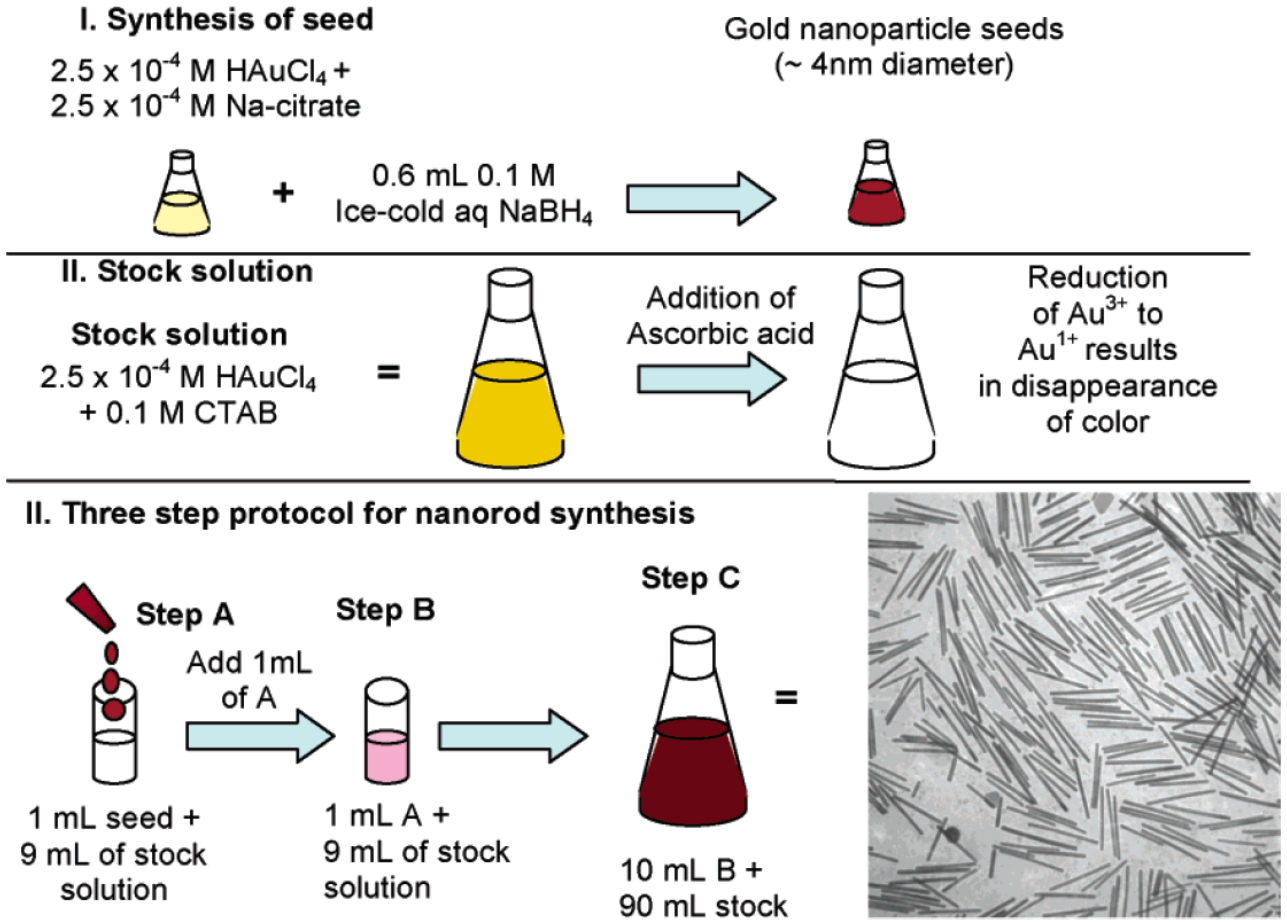

Figure 2. Seed-mediated growth approach to making gold and silver nanorods of controlled aspect ratio. The specific conditions shown here, for 20 mL volume of seed solution, lead to high-aspect ratio gold nanorods. (bottom right) Transmission electron micrograph of gold nanorods that are an average of 500 nm long.

J. Phys. Chem. B **2005,** *109,* 13857−13870

Directional Growth

Cetrimonium bromide ($(C_{16}H_{33})N(CH_3)_3Br$) (CTAB)

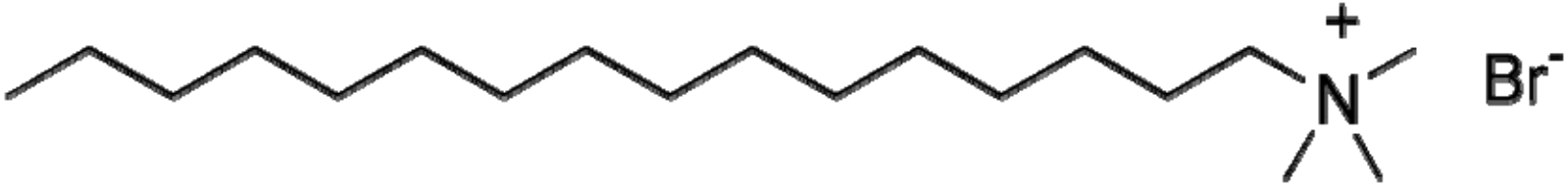

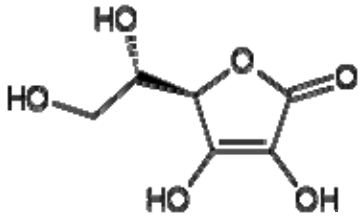

Ascorbic acid

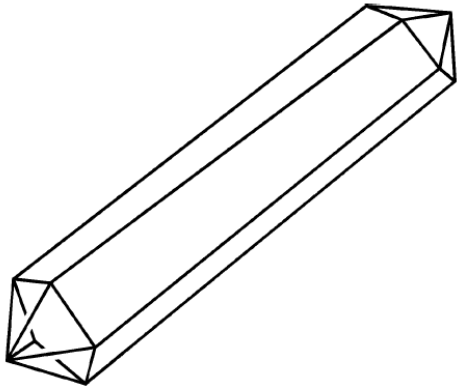

Figure 5. Cartoon of the crystallography of gold nanorods. The direction of elongation is [110]. The cross-sectional view is a pentagon; each end of the rod is capped with five triangular faces that are Au{111}. The sides of the rods are not as well-defined; either Au{100} or Au{110} faces, or both.

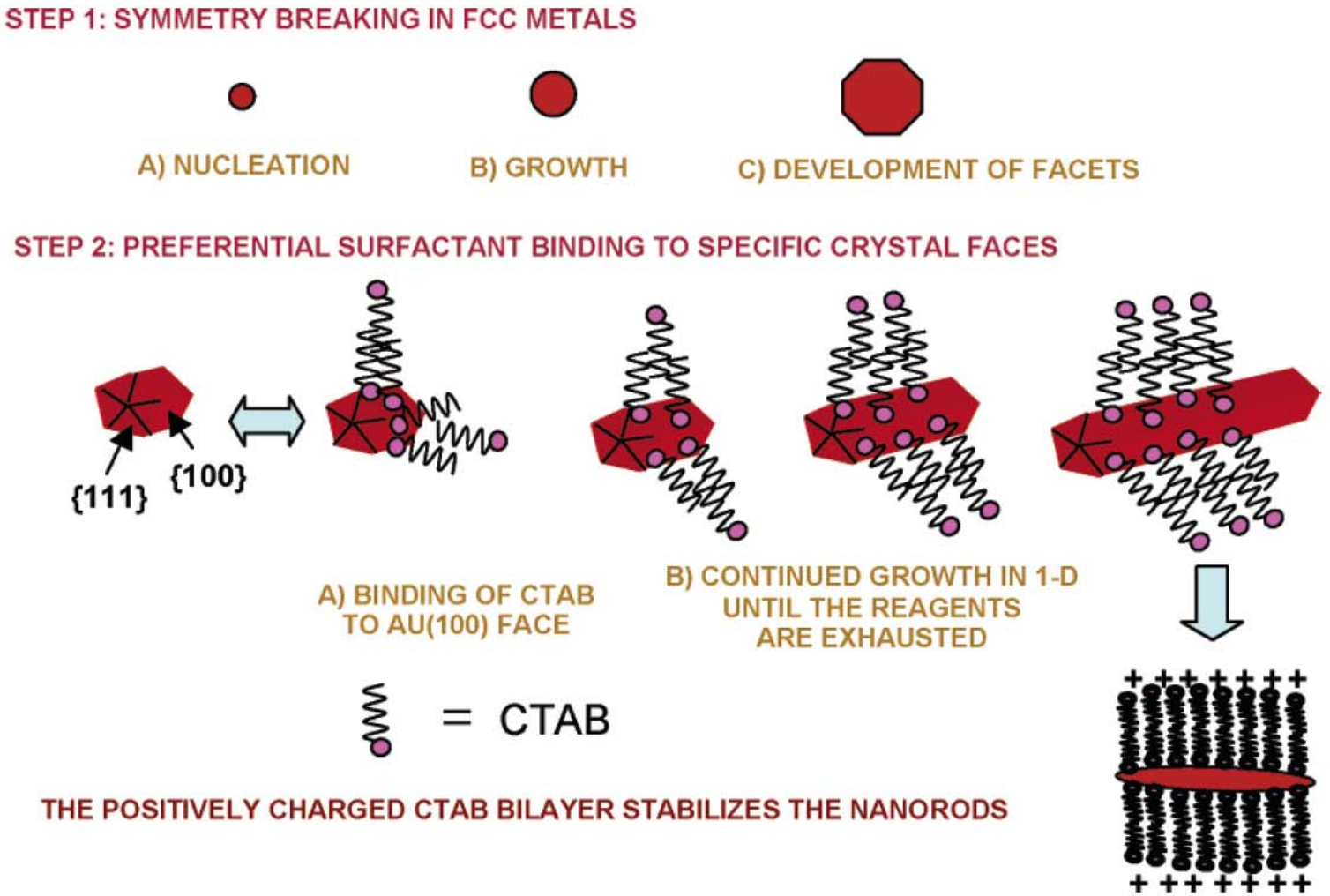

Figure 8. Proposed mechanism of surfactant-directed metal nanorod growth. The single crystalline seed particles have facets that are differentially blocked by surfactant (or an initial halide layer that then electrostatically attracts the cationic surfactant). Subsequent addition of metal ions and weak reducing agent lead to metallic growth at the exposed particle faces. In this example, the pentatetrahedral twin formation leads to Au {111} faces that are on the ends of the nanorods, leaving less stable faces of gold as the side faces, which are bound by the surfactant bilayer.

Nanorods

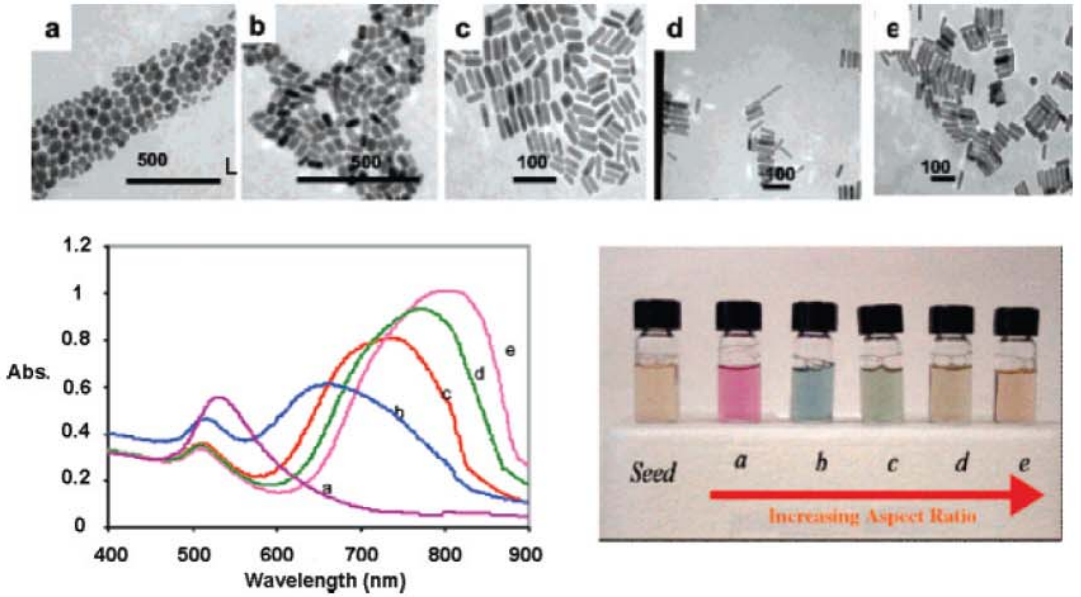

Figure 3. Transmission electron micrographs (top), optical spectra (left), and photographs (right) of aqueous solutions of Au nanorods of various aspect ratios. The seed sample has an aspect ratio of 1. Samples a, b, c, d, and e have aspect ratios of 1.35 ± 0.32, 1.95 ± 0.34, 3.06 ± 0.28, 3.50 ± 0.29, and 4.42 ± 0.23, respectively. Scale bars: 500 nm for a and b, 100 nm for c−e. Reprinted with permission from ref 16. Copyright 2005 American Chemical Society.

Nanocube and Nanorice

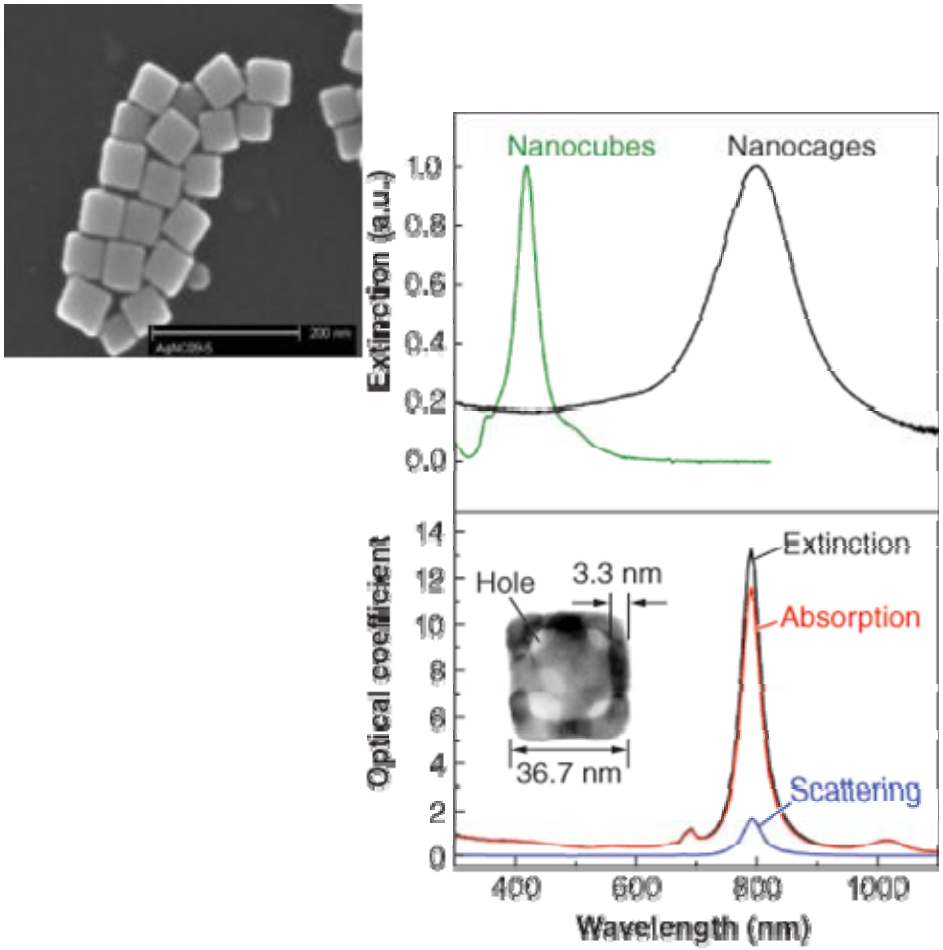

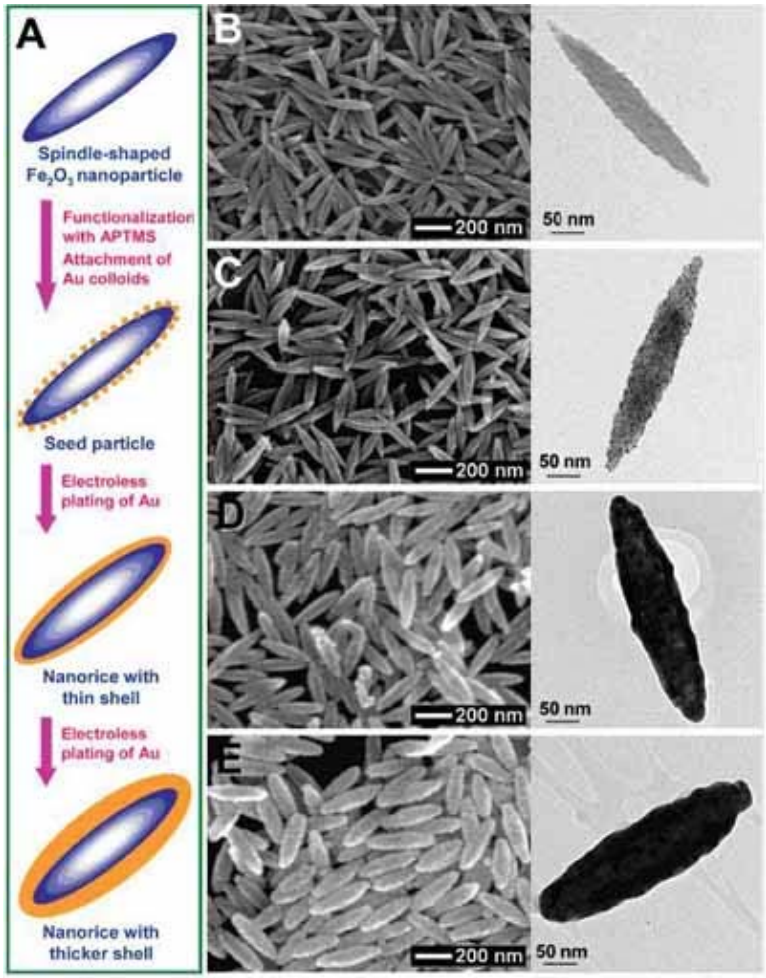

The graphic above depicts various magnitudes of nanorice, which is a rice-shaped nanoparticle with a non-conducting core made of iron oxide and covered by a metallic shell made of gold. Scientists plan to attach the nanorice to scanning probe microscopes to obtain very clear image quality that surpasses today's technology. For the Air Force, this technology could be used as a tool to develop new high-speed optoelectronic materials and to monitor chemical reactions. (Graphic provided by Prof. Naomi Halas)

Template Synthesis

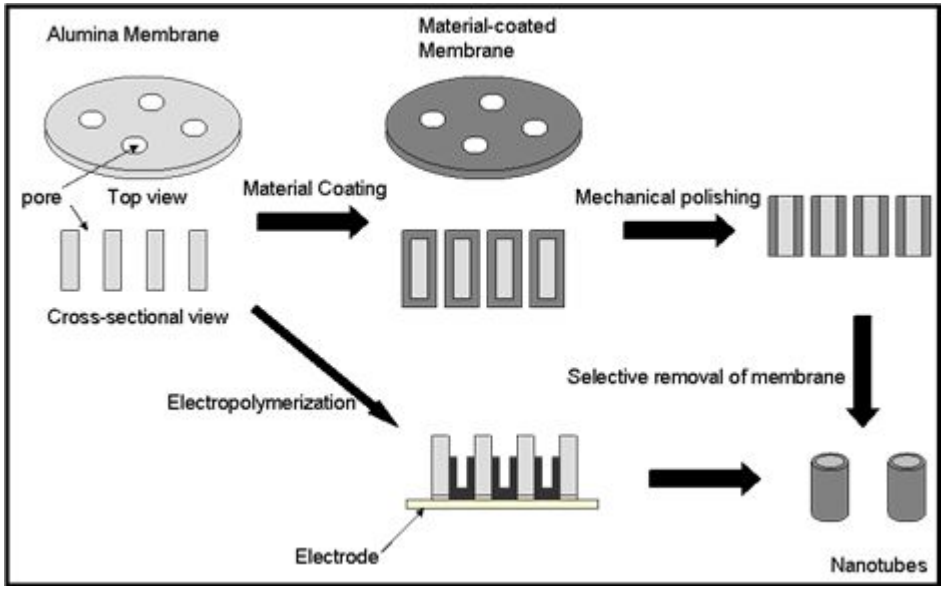

Porous Materials

- AAO
- MCM-41

- Micro-
- Meso
- Macro-

Polymer

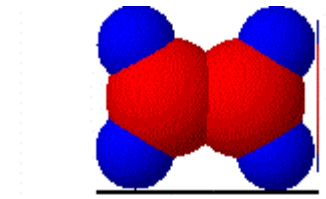

a monomer ethene

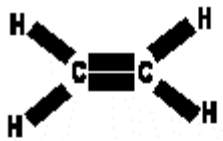

C_2H_4

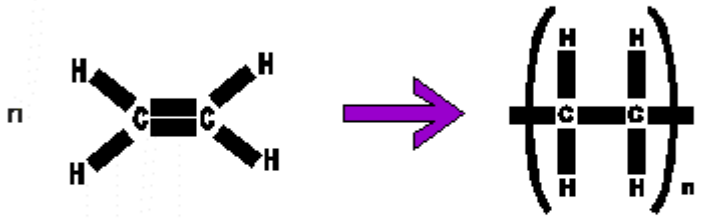

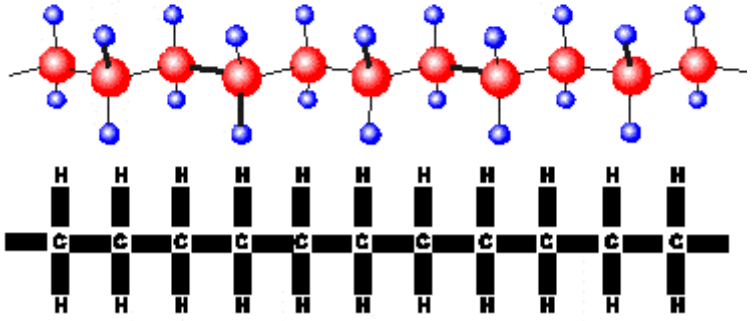

a polymer poly(ethene)

Block copolymer

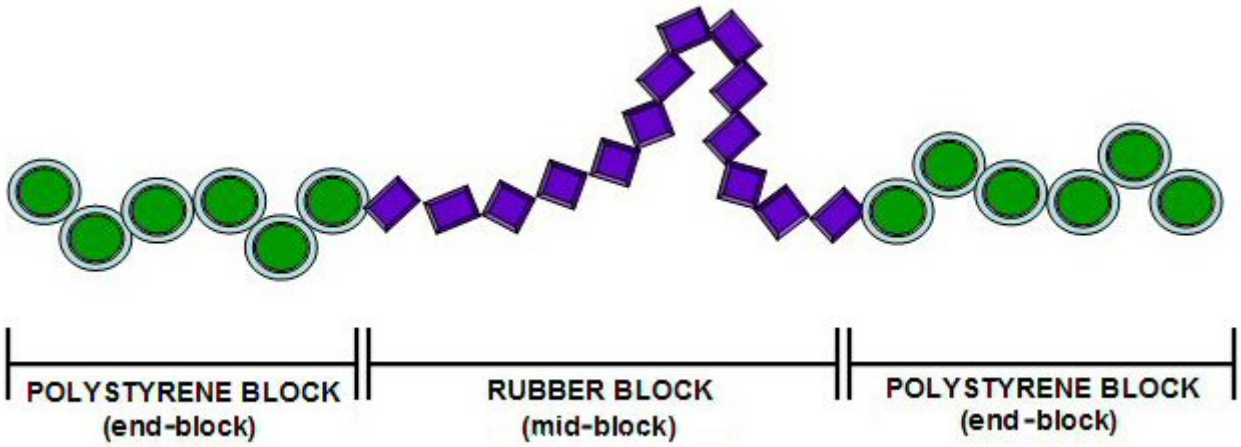

Phase Segregation

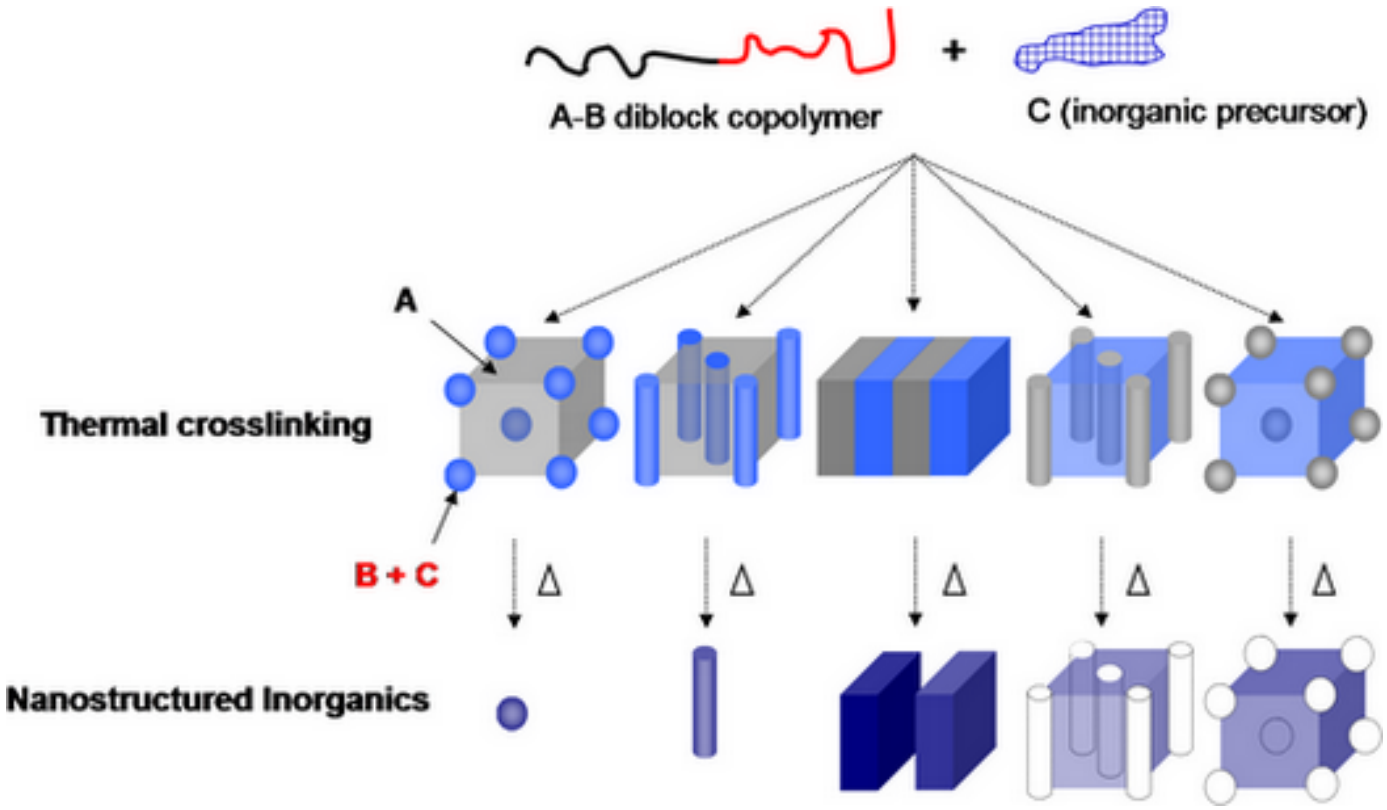

Surface Functionalization

- Recognition
  - Molecular Recognition
    - Protein
    - DNA
    - Saccharide
- Reporting/Detection
  - Dye
  - Quantum dots
  - SPR
  - SERS/LSPR
- Separation
  - Gel/Chromatography
  - Magnetic

- Surfaces
  - Gold and silver
  - Silicon oxide (glass)
  - Quantum dots
  - Polymer

Carboxyl Presenting Surfaces

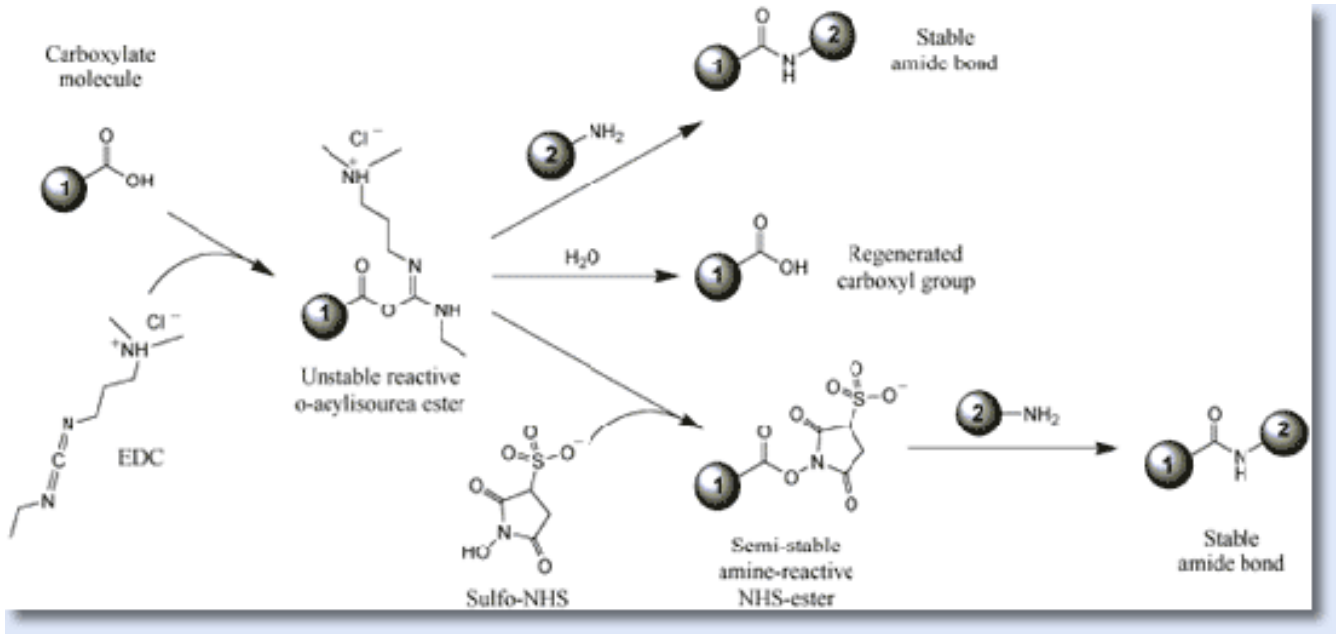

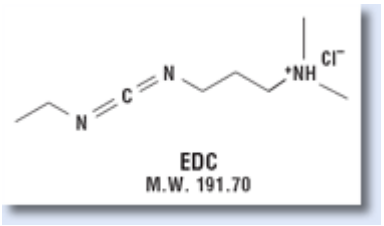

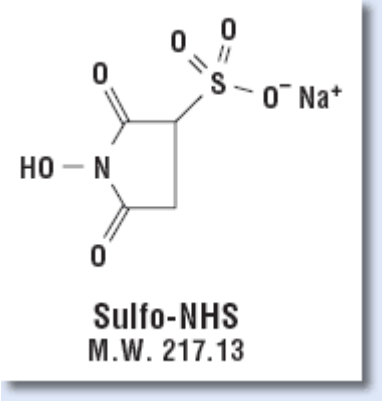

EDC (1-Ethyl-3-[3-dimethylaminopropyl]carbodiimide Hydrochloride)

Amine Presenting Surface

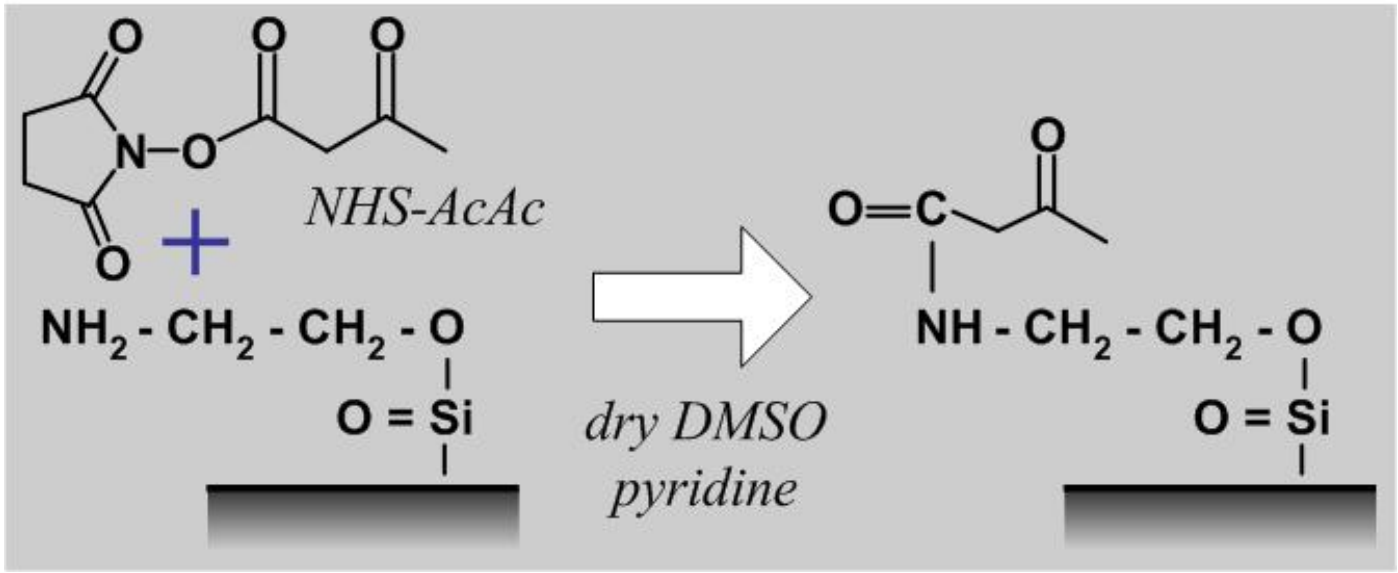

Sulfhydryl Labeling

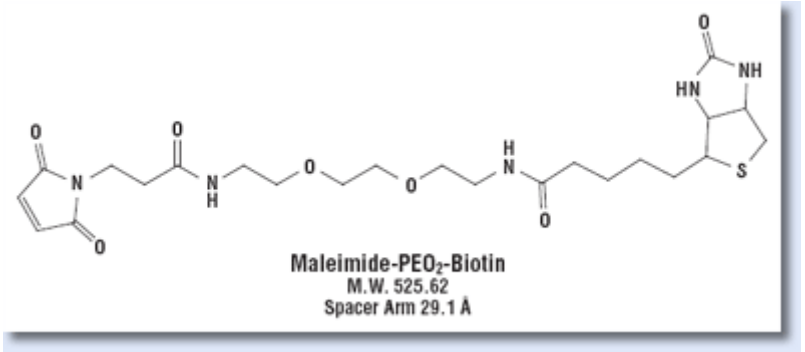

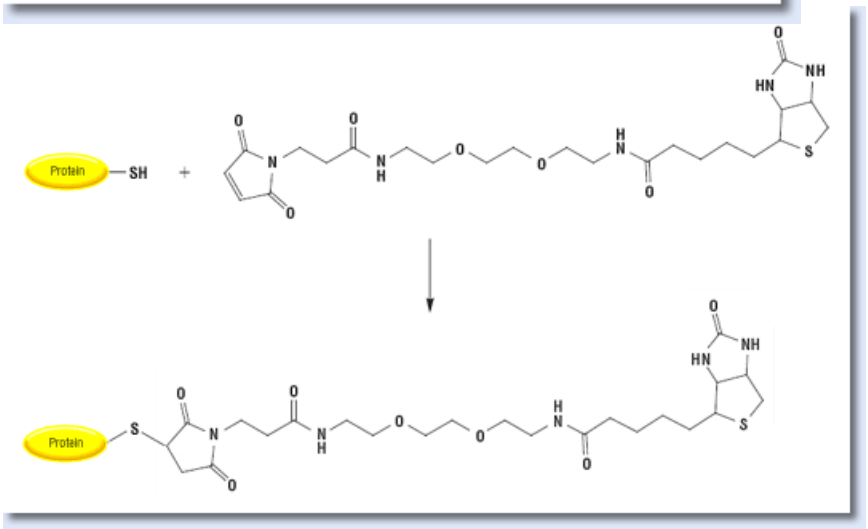

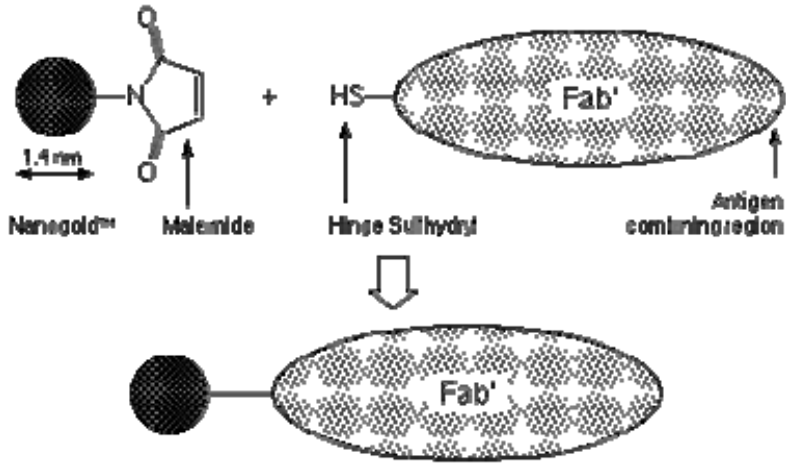

Silica Modification

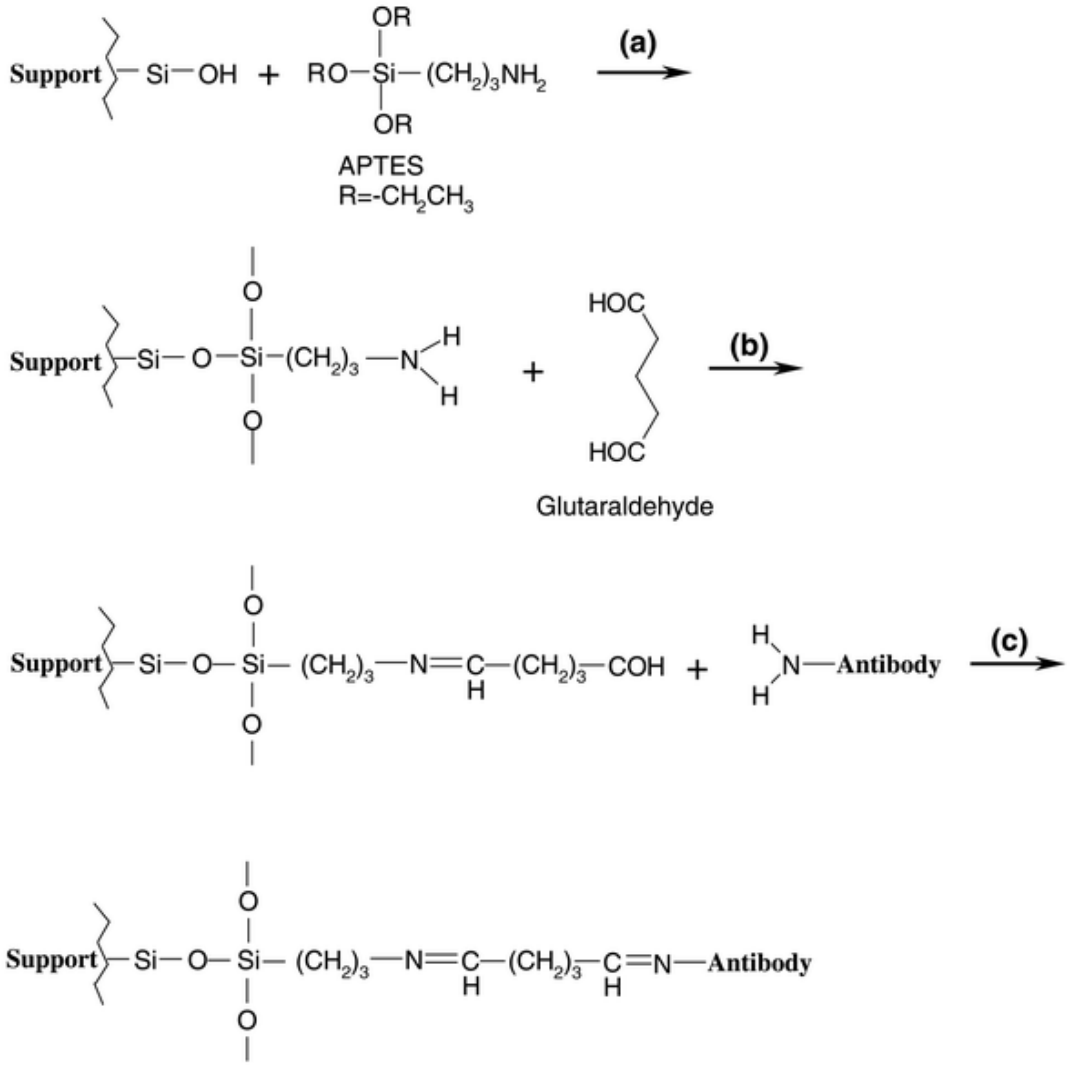

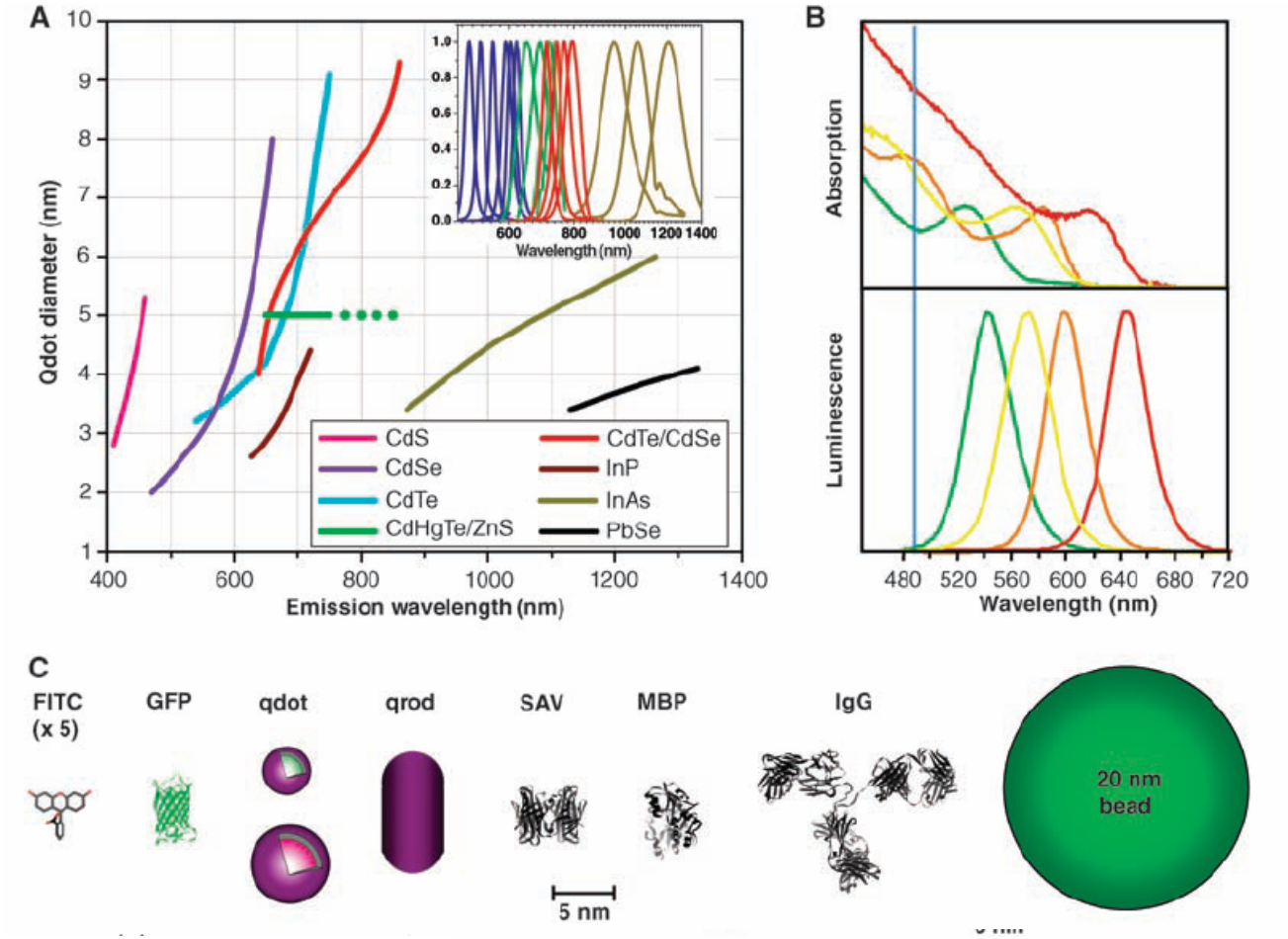

Fig. 1. (**A**) Emission maxima and sizes of quantum dots of different composition. Quantum dots can be synthesized from various types of semiconductor materials (II-VI: CdS, CdSe, CdTe…; III-V: InP, InAs…; IV-VI: PbSe…) characterized by different bulk band gap energies. The curves represent experimental data from the literature on the dependence of peak emission wavelength on qdot diameter. The range of emission wavelength is 400 to 1350 nm, with size varying from 2 to 9.5 nm (organic passivation/solubilization layer not included). All spectra are typically around 30 to 50 nm (full width at half maximum). Inset: Representative emission spectra for some materials. Data are from (*12*, *18*, *27*, *76*–*82*). Data for CdHgTe/ZnS have been extrapolated to the maximum emission wavelength obtained in our group. (**B**) Absorption (upper curves) and emission (lower curves) spectra of four CdSe/ZnS qdot samples. The blue vertical line indicates the 488-nm line of an argon-ion laser, which can be used to efficiently excite all four types of qdots simultaneously. [Adapted from (*28*)] (**C**) Size comparison of qdots and comparable objects. FITC, fluorescein isothiocyanate; GFP, green fluorescent protein; qdot, green (4 nm, top) and red (6.5 nm, bottom) CdSe/ZnS qdot; qrod, rod-shaped qdot (size from Quantum Dot Corp.'s Web site). Three proteins—streptavidin (SAV), maltose binding protein (MBP), and immunoglobulin G (IgG)—have been used for further functionalization of qdots (see text) and add to the final size of the qdot, in conjunction with the solubilization chemistry (Fig. 2).

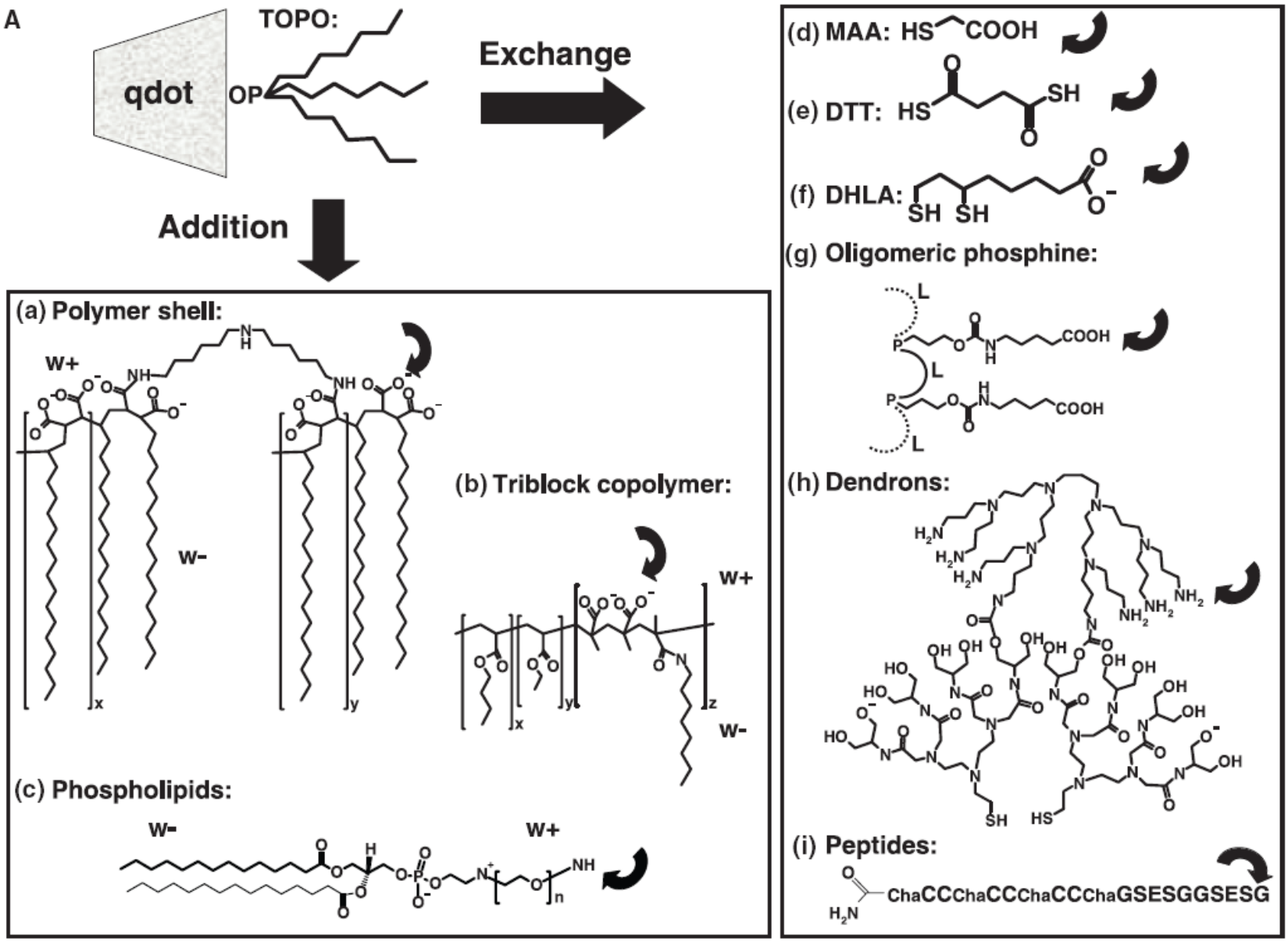
A
TOPO:
qdot
OP
Exchange
Addition
(a) Polymer shell:
W+
W-
(b) Triblock copolymer:
W+
W-
(c) Phospholipids:
W-
W+
(d) MAA: HS COOH
(e) DTT: HS SH
(f) DHLA: SH SH
(g) Oligomeric phosphine:
COOH
COOH
(h) Dendrons:
(i) Peptides:
ChaCCChaCCChaCCChaGSESGGSESG

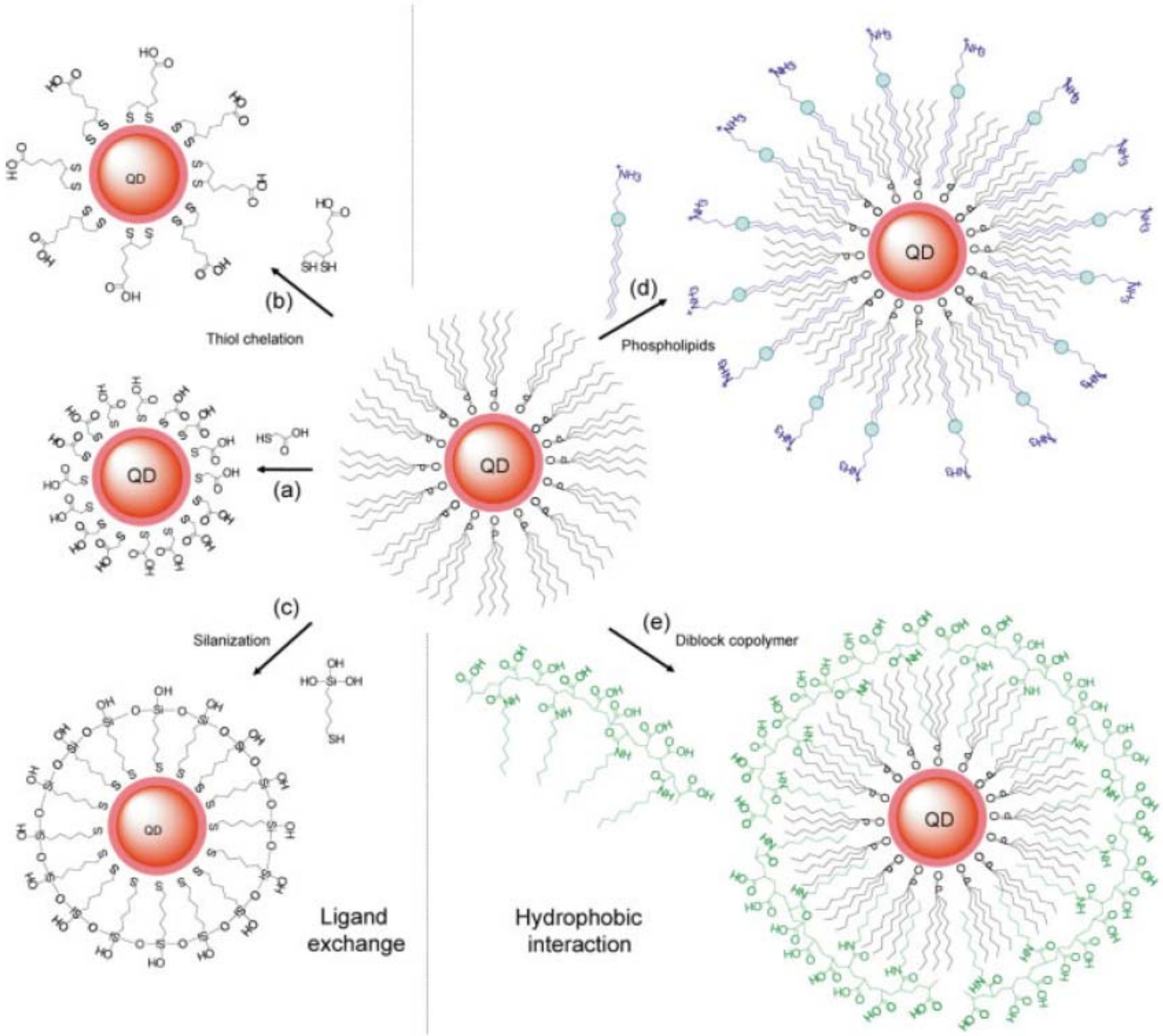
QD
(a)
(b)
Thiol chelation
(c)
Silanization
Ligand exchange
(d)
Phospholipids
(e)
Diblock copolymer
Hydrophobic interaction

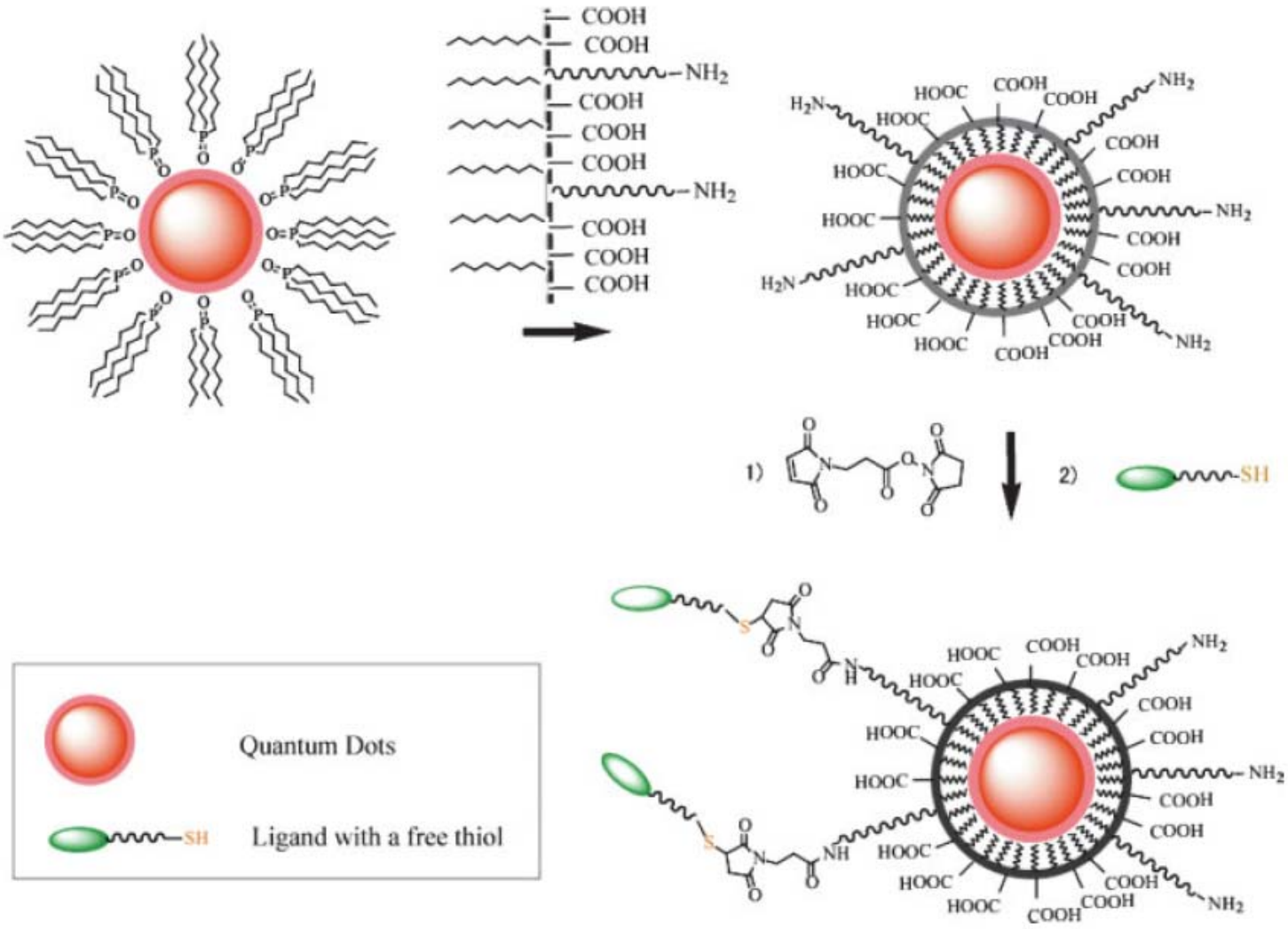

FIGURE 3 Maleimide functionalized QDs for conjugating thiol-containing ligands. TOPO stabilized QDs are coated with a primary amine functionalized tri-block amphiphilic copolymer for producing water-soluble QDs, which facilitate further conjugation to ligands with free thiols through bi-functional cross-linkers.

Cells incubated with tiopronin coated QDs

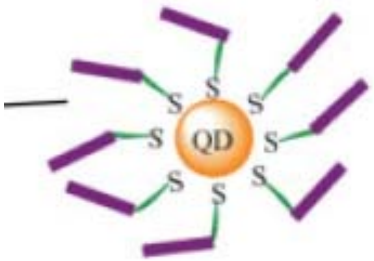

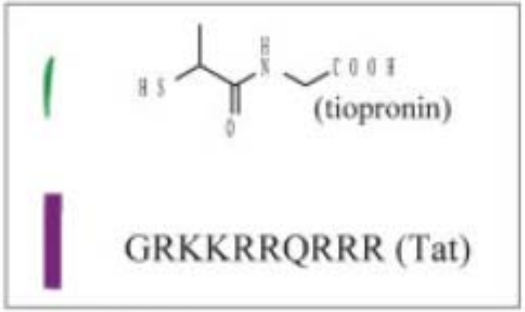

Cells incubated with Tat functionlized QDs

Scheme 1. Modular Design of Hydrophilic Ligands with Terminal Functional Groups Used in This Study